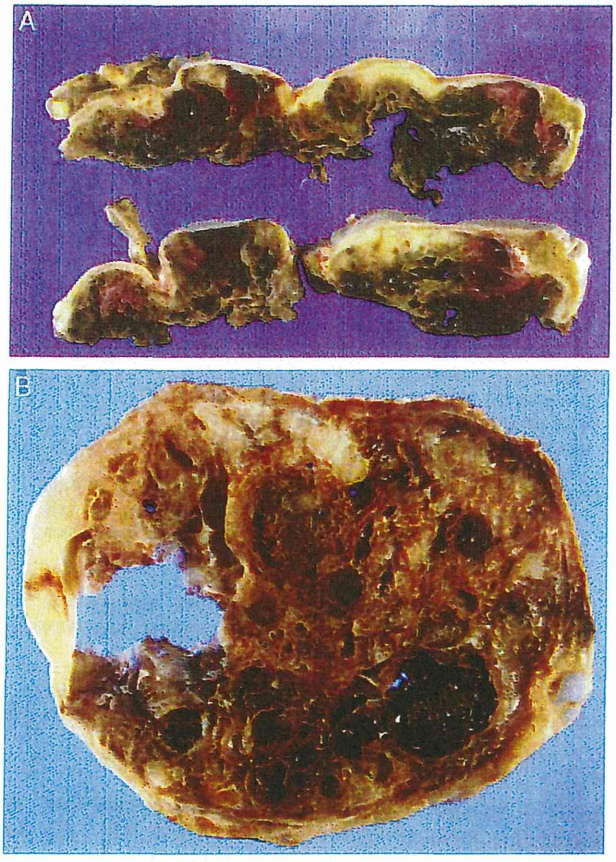

FIGURE 1. Gross pictures of ovarian MCST. A, Case 1. Cut section of the tumor showed solid and white areas admixed with numerous cystic lumens. Marked hemorrhagic changes were seen. B, Case 2. The cut surface of the tumor revealed a characteristic sponge-like appearance. Many of the cystic cavities were filled with bloody content. Whitish solid components were also present in the tumor.

variable sizes anastomosed with each other. The lumens of microcysts or macrocysts were filled with eosinophilic exudative content, myxoid content, or blood. Marked congestive changes were found in the tumor of case 2, and many of the cystic spaces lined by the tumor cells were filled with blood. These congestive areas gave a "hemangiomatous" or "hemangiopericytomatous" impression. Although many of the microcysts and macrocysts were lined by tumor cells, epithelial glandular differentiation was not evident in either of the tumors. Pseudopapillary architecture was absent in both tumors.

Individual tumor cells had round-to-ovoid and sometimes short-spindled nuclei with very fine chromatin. Nucleoli were inconspicuous or very small when present. Most of the neoplastic cells had a faintly eosinophilic cytoplasm. In general, tumor cell nuclei were monotonous and bland. However, in case 2, neoplastic cells with enlarged nuclei and abundant eosinophilic cytoplasm were observed focally in $< 1\%$ of the tumor. Some of these cells mimicked luteinized cells. Mitoses were hardly detected in either tumor (average: 0 mitoses/10 high-power field).

Immunophenotypes of Ovarian MCSTs, Other Ovarian Tumors, and Pancreatic SPNs

The 2 ovarian MCSTs examined in this study showed quite similar immunophenotypes. Diffuse and strong immunoreactivity for vimentin (Fig. 4A) and CD10 (Fig. 4B) was observed in both cases. In addition, we found that these tumors commonly showed diffuse and strong nuclear immunoreactivity for β-catenin (Fig. 5A) and Wilms tumor 1 (WT-1) (Fig. 4C). MCSTs were completely negative for sex cord markers (α-inhibin and calretinin), hormone receptors (estrogen receptor and progesterone receptor), neuroendocrine markers (CD56, synaptophysin, and chromogranin A), vascular markers (CD31, CD34, and D2-40), and mesenchymal markers including desmin and smooth muscle actin. Other negative markers included CD99, thyroid transcription factor-1, α-fetoprotein, SALL4, epithelial membrane antigen, cytokeratin (Cam 5.2), and cytokeratin 7. MCST in case 1 was completely negative for cytokeratin (AE1/AE3). However, approximately 20% of the tumor cells in case 2 showed positive immunoreactivity for cytokeratin (AE1/AE3) (Fig. 4D). Ki-67-labeling index (MIB-1 index) was 7% and 10% in case 1 and case 2, respectively.

Immunophenotypes of ovarian MCSTs, other ovarian tumors that can exhibit similar morphologic features, such as sex cord-stromal tumors, SOs, and YSTs, and pancreatic SPNs, are summarized in Table 2. Among the ovarian tumors examined, aberrant nuclear accumulation of β-catenin was specifically observed in MCSTs (Figs. 6B–E). Two of 3 pancreatic SPNs showed nuclear immunoreactivity for β-catenin (Fig. 6F). Vimentin was expressed in most ovarian sex cord-stromal tumors. In contrast, CD10 positivity was rarely observed in ovarian sex cord-stromal tumors, YSTs, or SOs. Although WT-1 expression was commonly observed in various kinds of ovarian sex cord-stromal tumors, including GCTs, fibromas, thecomas, and Sertoli-Leydig cell tumors, their immunoreactivity was usually neither as strong nor as diffuse in comparison with WT-1 expression in MCSTs. α-Inhibin, which is frequently expressed in ovarian sex cord-stromal tumors, was not expressed in MCSTs. The pancreatic SPNs were positive for CD10 and vimentin. However, we observed a significant difference in the immunophenotypes of MCSTs and SPNs, with MCSTs showing a $WT\text{-}1^{+}/PgR^{-}/CD56^{-}$ pattern and SPNs showing a $WT\text{-}1^{-}/PgR^{+}/CD56^{+}$ pattern.

Mutation Analyses of β-catenin (CTNNB1) and FOXL2 in MCSTs

Both cases of ovarian MCST had the same oncogenic missense mutations of *CTNNB1*, which is the gene encoding β-catenin (Fig. 4). The mutations detected were both c.98C > G mutations that cause replacement of serine with cysteine at codon 33. Mutations in exon 1 of *FOXL2* were not detected in MCSTs.

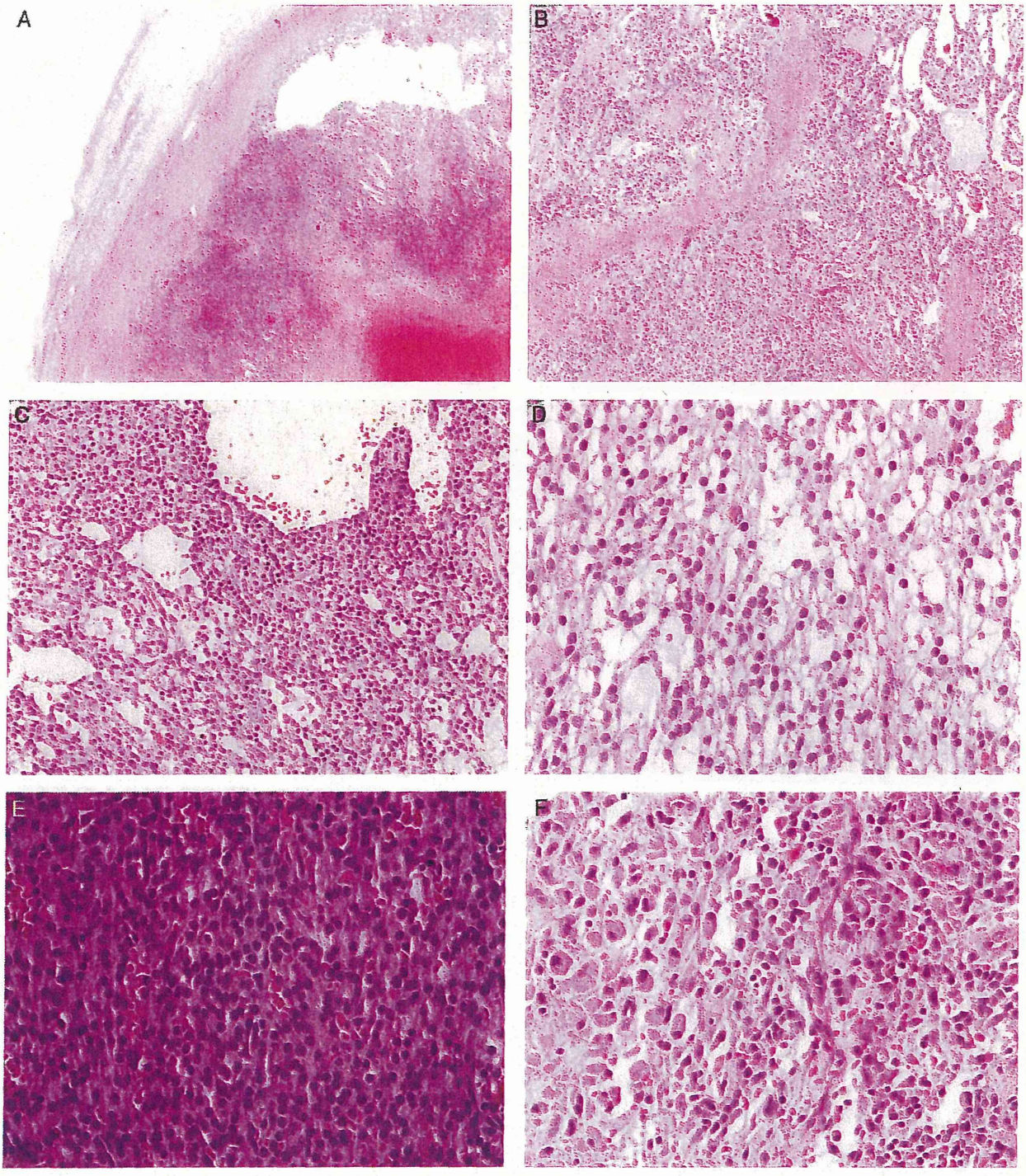

FIGURE 2. Histology of ovarian MCST in case 1. A, Low-power view of the tumor. The tumor was a well-demarcated lesion with a fibrous capsule. Marked hemorrhage was observed in its center. B, Thick fibrous stroma was seen between areas of tumor cell growth. C, Tumor cells formed cysts of various sizes. A mixture of microcystic and macrocystic structures was observed. D, Representative high-power view of the tumor. Monotonous and bland tumor cells with round-to-ovoid nuclei grew in a microcystic pattern. E, A solid pattern of growth was seen in parts. F, Some tumor cells had abundant eosinophilic cytoplasm.

DISCUSSION

In this study, we describe the histopathologic features of ovarian MCSTs in detail. Although the number of cases we studied was not large, their unique and impressive histology and homologous immunophenotype convinced us of their distinct nature among

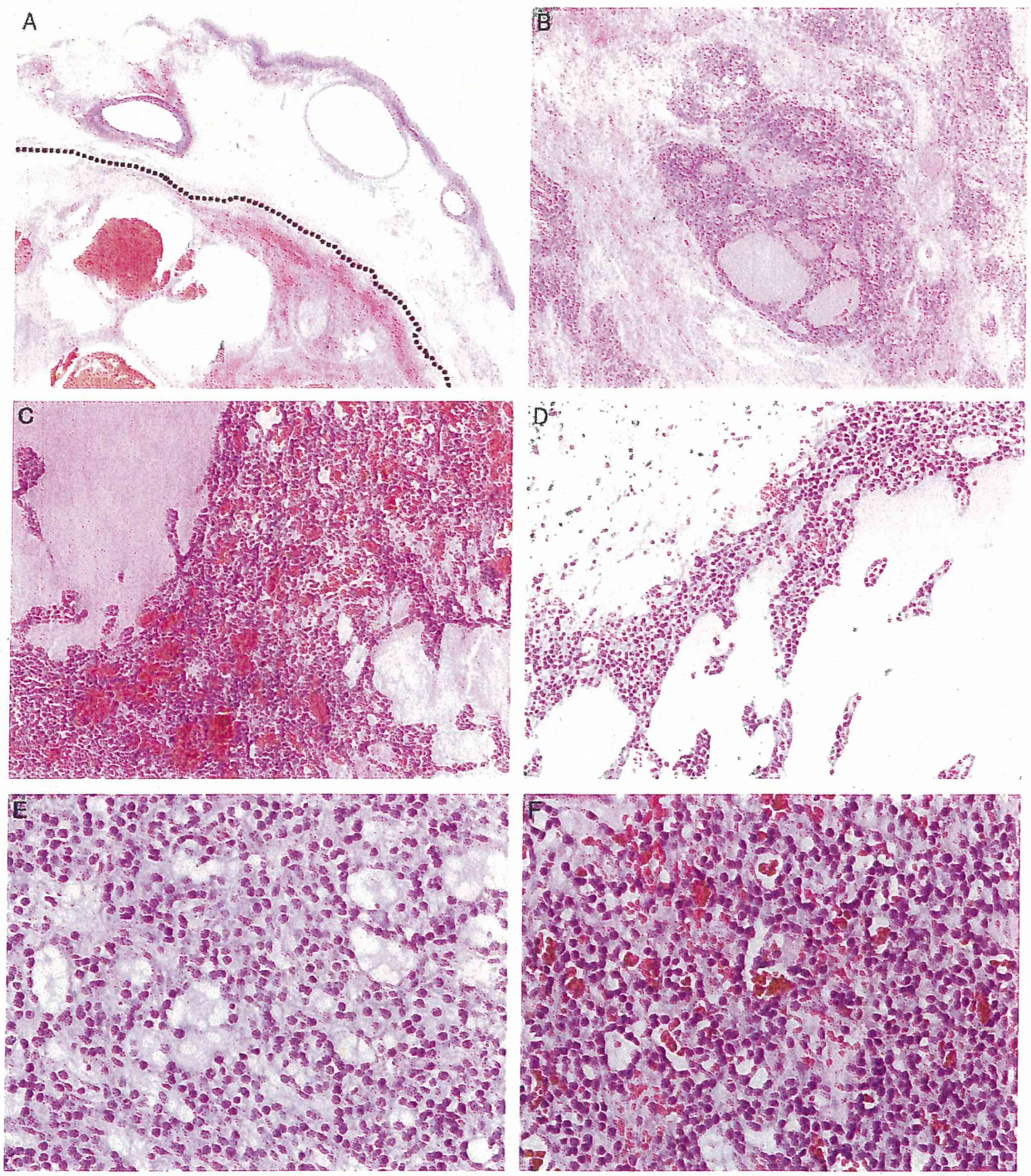

FIGURE 3. Histology of ovarian MCST in case 2. A, Low-power view of the tumor border (dotted line). A thin layer of ovarian medulla was seen surrounding the tumor. The ovarian cortex was well preserved, and numerous follicles could be seen. B, Tumor cell nests and intersecting fibrous stroma. C, The tumor cells grew in macrocystic and microcystic patterns. Marked congestion was observed. D, The wall of the macrocystic space was lined with irregularly shaped nests of tumor cells. E, Representative high-power view of the tumor. Cells with minimum cytologic atypia grew in microcystic and solid patterns. F, Hemangiomatous component of the tumor. The cystic lumens were filled with blood.

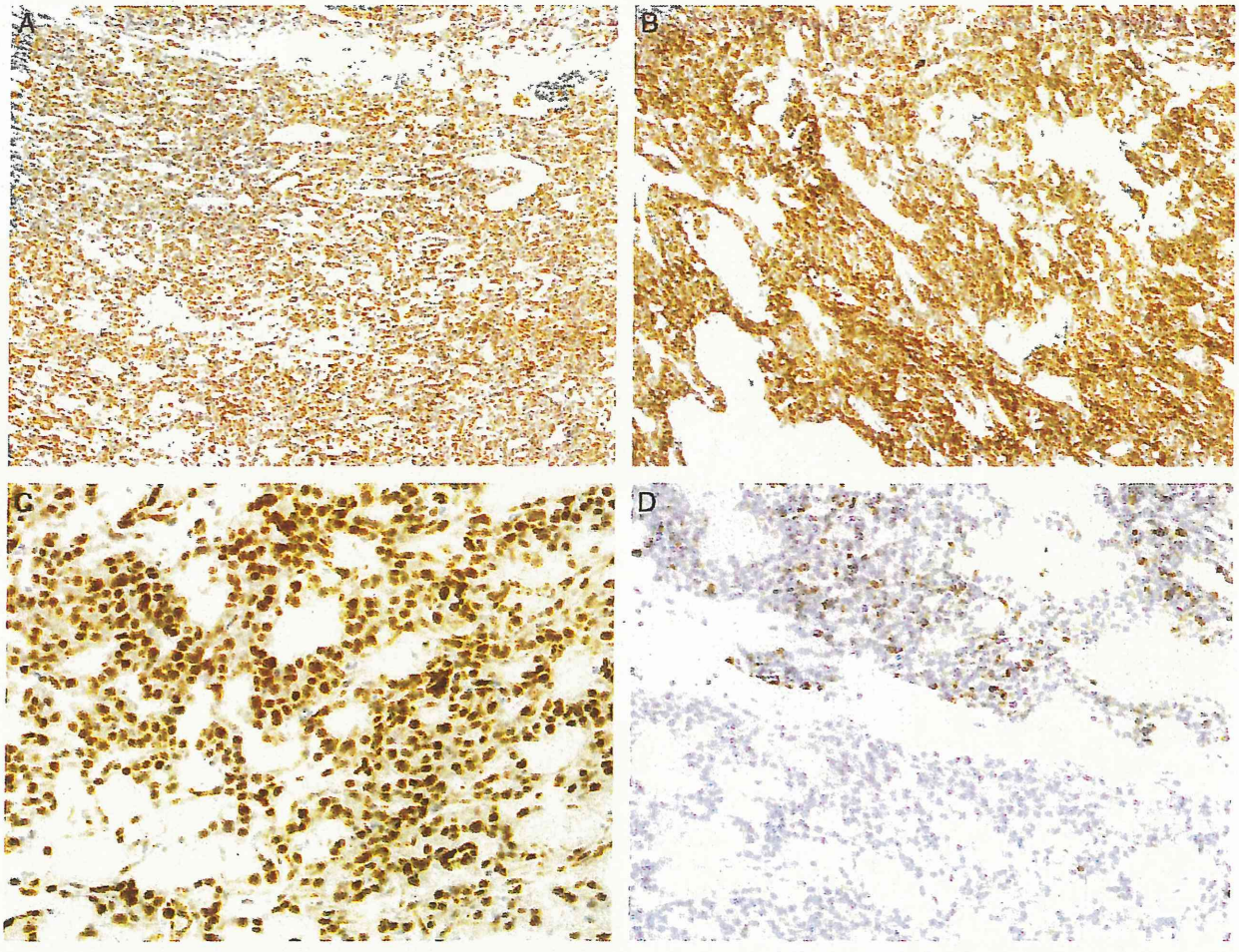

FIGURE 4. Immunohistochemical features of ovarian MCSTs. Both cases of ovarian MCSTs showed diffuse and strong positivity for (A) vimentin, (B) CD10, and (C) WT-1. D. In case 2, the tumor showed focal staining for cytokeratin (AE1/AE3).

ovarian neoplasms and prompted us to further investigate their pathogenesis.

Macroscopically, ovarian MCSTs in our series commonly showed a "solid and cystic" or "sponge-like" appearance. In a previously reported series,[7] 11 of 16 MCSTs showed a solid and cystic gross appearance, and 2 cases were predominantly cystic. Thus, we believe that a "solid and cystic" gross appearance is one of the key features of MCSTs.

Histologically, the following features appear to be characteristic of MCSTs:

1. Mixture of microcystic, macrocystic, and solid structures.
2. Presence of intervening thick fibrous stroma.
3. Growth of monotonous tumor cells with round-to-ovoid and generally bland nuclei with very fine chromatin.
4. Well-demarcated tumor borders.
5. Focal areas of congestive and hemorrhagic change that can give a hemangiomatous impression.

In a previous report,[7] the researchers primarily focused on the microcystic pattern as the characteristic structural pattern of MCSTs. The microcystic feature was observed in all of their cases and was regarded as the most striking morphologic characteristic. This was the main reason why they included "microcystic" in the nomenclature when proposing this new and unique ovarian tumor entity. Along with the microcystic pattern, a solid pattern of tumor cell growth was described in their report. Notably, microcystic components were relatively minor in some of their cases. In our cases, the tumors were composed mainly of 3 major structural patterns: "microcystic," "macrocystic," and "solid." Although the macrocystic structure was not described in the previous series, it was commonly observed in our cases and was predominant in 1 case. Therefore, we believe that it should be listed as one of the major structural patterns that MCSTs exhibit. At this point, it is unclear how microcysts and macrocysts are formed in MCSTs. Whether it is the nature of tumor cells to form cysts, or cystic spaces are the consequence of degenerative changes, is unknown. Many of the cystic spaces are, in fact, lined by tumor cells. However, epithelial glandular differentiation (glands formed by cuboidal cells or columnar cells)

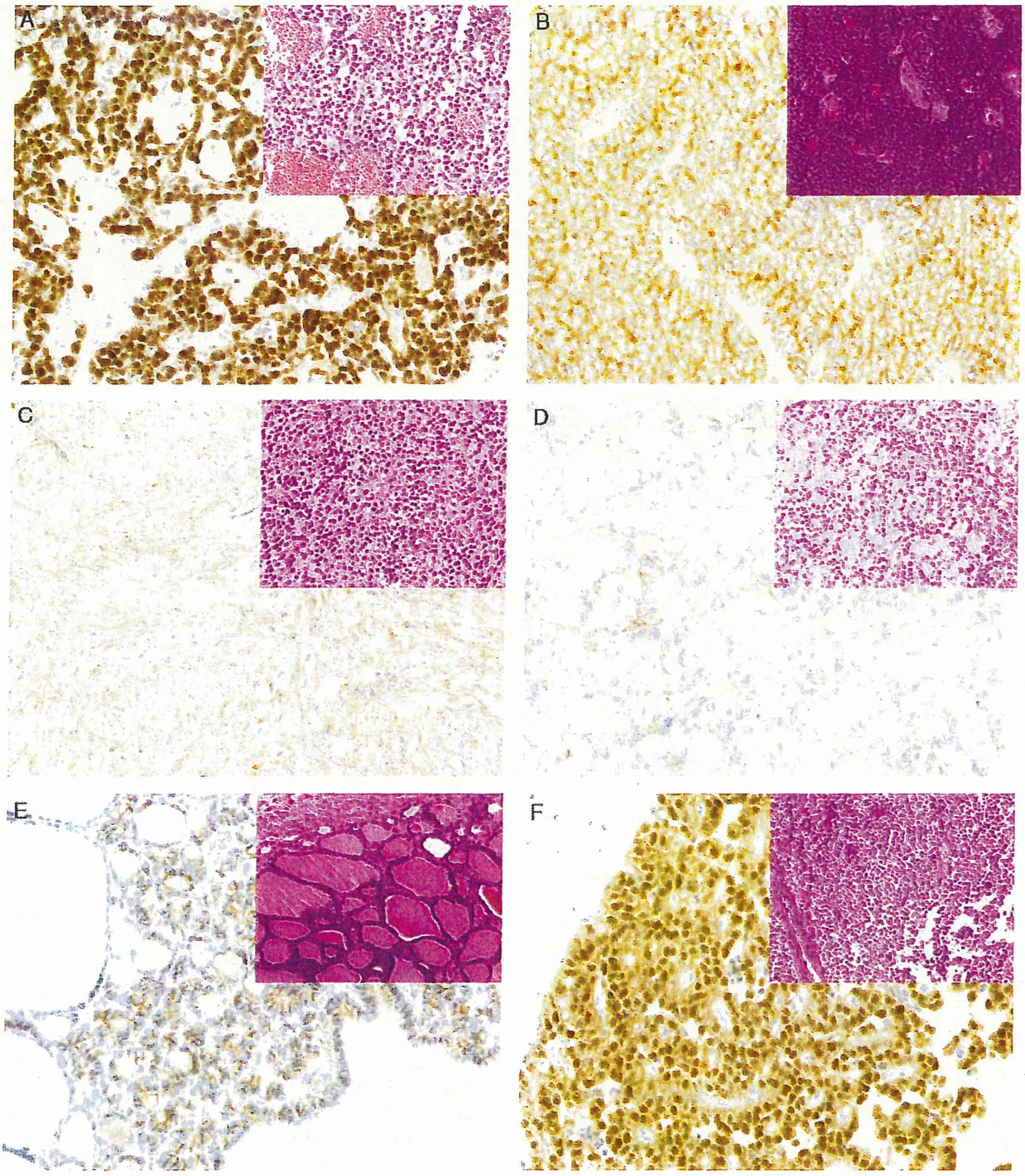

FIGURE 5. Immunohistochemical detection of β-catenin protein in ovarian (A) MCST, (B) AGCT, (C) thecoma, (D) YST, (E) SO, and (F) pancreatic solid pseudopapillary tumor. Among the ovarian tumors examined in this series, diffuse nuclear accumulation of β-catenin protein was observed only in MCST. Pancreatic SPN showed a similar expression pattern.

was not observed in any areas of the tumor. A gradual transition between solid, microcystic, and macrocystic areas was observed, and contents of the cystic lumen differed significantly from exudative, myxoid, to bloody. On the basis of these findings, we speculate that stromal alteration caused by tumor cell secretion or degenerative changes due to processes such as edema and congestion play a role in the formation of variably sized cystic lumens in MCSTs.

In addition to the above described structural patterns, the nuclear features of MCSTs are also

TABLE 2. Results of Immunohistochemistry in Ovarian MCSTs, Other Ovarian Tumors, and Pancreatic SPNs

	Ovary						Pancreas
	MCST	GCT	F/T/FT	Other SCST	YST	SO	SPN
β-Catenin	2/2	0/13	0/19	0/6	0/8	0/7	2/3
CD10	2/2	0/13	1/19	2/6	1/8	2/7	3/3
Vimentin	2/2	13/13	19/19	6/6	6/8	7/7	3/3
WT-1	2/2	8/13	15/19	2/6	0/8	0/7	0/3
α-Inhibin	0/2	12/13	7/19	6/6			
TTF-1	0/2					7/7	
SALL4	0/2				8/8		
AFP	0/2				8/8		
PgR	0/2						3/3
CD56	0/2						3/3

AFP indicates α-fetoprotein; F, fibroma; FT, fibrothecoma; PgR, progesterone receptor; SCST, sex cord-stromal tumor; T, thecoma; TTF-1, thyroid transcription factor 1.

characteristic. The nuclei are round to ovoid and, for the most part, "monotonous." The chromatin pattern is very fine. Nucleoli are not prominent, and nuclear grooves are rarely observed. In general, nuclear pleomorphism is minimal. Despite the fact that foci of bizarre nuclei were reported in more than half of the cases in previous series, they were distributed in a patchy/random manner and comprised $<5\%$ to 10% of overall tumor volume.[7] Tumor cells with hyperchromatic and enlarged nuclei were present in case 1 of our series; however, it only made up $<1\%$ of the whole tumor volume.

Histologic features of MCST such as well-demarcated tumor border, generally bland and monotonous nuclear feature, and low mitotic activity are suggestive of the benign or nonaggressive nature of MCSTs. Clinical behavior of the previous reported MCST cases was favorable.[7] All patients with follow-up information were alive and without evidence of disease. In our series, both tumors were confined in the ovaries at the time of surgery. No distant metastases or peritoneal spread was detected during the follow-up period. However, the number of reported MCSTs is still small, and their follow-up periods are mostly short. Therefore, further studies in larger numbers of cases are necessary to reach definitive conclusions with regard to the behavior and prognosis of MCST.

Immunohistochemical analysis of ovarian MCSTs revealed a characteristic pattern. In addition to diffuse and strong positivity for vimentin and CD10 as reported previously,[7] we found that MCSTs commonly show diffuse nuclear immunoreactivity for β-catenin and WT-1. In general, vimentin and CD10 are of limited use in diagnosing ovarian tumors when each is used as a single marker. Vimentin is positive in various kinds of sex cord-stromal tumors,[16,19,25] endometrioid tumors,[4,6] and mesenchymal tumors.[9,12] CD10 positivity has also been reported in many pure stromal and sex cord-stromal tumors of the ovary.[15] In fact, occasional CD10 positivity was seen in various sex cord-stromal tumors, YSTs, and SOs in our series. However, an ovarian neoplasm that expresses nuclear β-catenin and WT-1, in combination with CD10 and vimentin, is unique. Therefore, we regard this vimentin$^+$/CD10$^+$/WT-1$^+$/β-catenin$^+$ immunophenotype as another key feature that characterizes ovarian

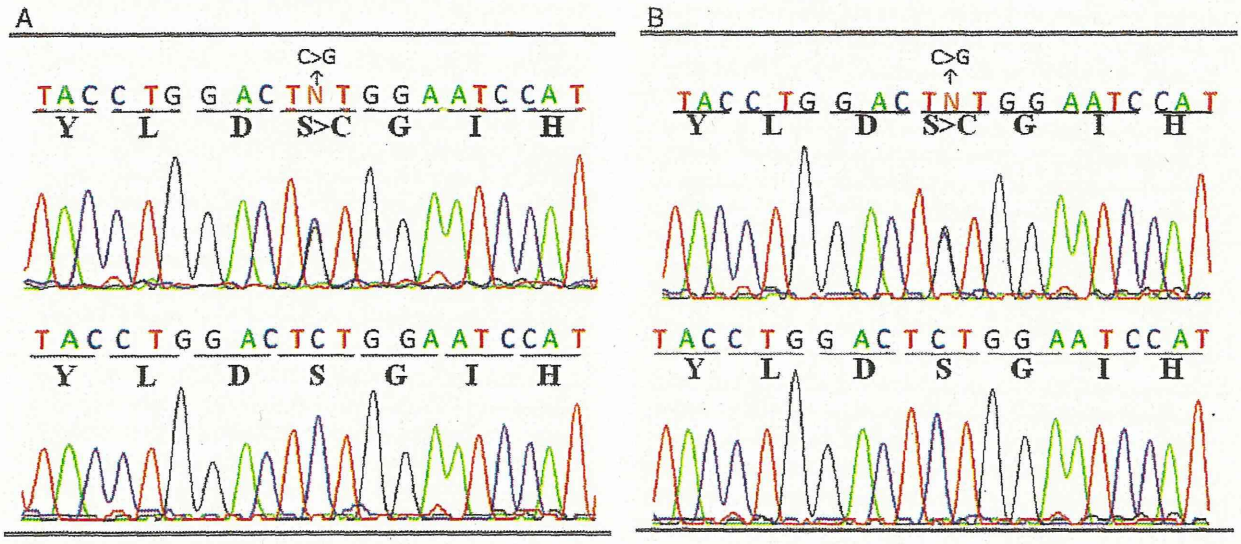

FIGURE 6. In these sequencing chromatograms, the top panel is from MCST, and the bottom panel is the corresponding control sequence. Both cases of ovarian MCST had an oncogenic missense *β-catenin* (*CTNNB1*) mutation, c.98C>G (A: case 1; B: case 2). This mutation causes replacement of serine with cysteine at codon 33, thereby leading to loss of a GSK3β phosphorylation site in the β-catenin protein. C indicates cysteine; D, aspartic acid; G, glycine; H, histidine; I, isoleucine; L, leucine; S, serine; Y, tyrosine.

MCSTs. Consistent with previous reports,[7] the MCSTs in our series were negative for sex cord-stromal markers such as α-inhibin and calretinin. With regard to epithelial markers, focal cytokeratin (Cam 5.2) positivity was reported in 4 of 16 cases in the previous series.[7] In our series, neither of the tumors expressed cytokeratin (Cam 5.2). However, 1 of the cases showed focal positivity for cytokeratin (AE1/AE3).

Much remains unclear regarding the origin of ovarian MCST. Irving and Young[7] suggested a possible stromal origin by excluding other possibilities. We agree that MCST does not fit into the category of surface epithelial stromal tumors or germ cell tumors. Morphologically, these tumors give the impression of stromal or mesenchymal origin, and positive immunoreactivity for vimentin may support the stromal/mesenchymal origin. However, cytokeratin immunoreactivity observed in approximately half of the MCSTs in the previous report and in this study leaves room for a pluripotent nature of the tumor cells. Therefore, on the basis of current evidence, we believe that it is more appropriate to regard MCSTs as "unclassifiable" or as "tumors of uncertain origin" than to classify them as conventional sex cord-stromal tumors.

In this study, we examined β-catenin alterations to understand the pathogenesis of MCSTs. Initially, one of the authors (J.S.) who is a specialist in hepatopancreaticobiliary pathology found morphologic and immunohistochemical similarities between the tumor in case 1 and pancreatic SPN. Monotonous growth of tumor cells with round-to-ovoid, sometimes spindled, nuclei is commonly found in ovarian MCSTs and pancreatic SPNs. Solid areas of ovarian MCST closely resemble those of pancreatic SPN, despite the fact that microcystic changes are usually not present in SPN, and pseudopapillary structures were absent in our MCSTs. Further, diffuse immunoreactivity for CD10 and vimentin is observed both in ovarian MCSTs[7] and pancreatic SPNs.[14] Pancreatic SPN is generally recognized as an epithelial tumor of the pancreas that arises almost exclusively in young women. It is well known for showing aberrant nuclear β-catenin expression that can be detected by immunohistochemistry.[24] In addition, mutations in exon 3 of the *β-catenin* gene are frequently detected in pancreatic SPNs.[1,24] Therefore, we sought to determine whether ovarian MCST shows aberrant nuclear β-catenin expression.

The significance of nuclear β-catenin accumulation in ovarian MCSTs cannot be overemphasized, because it directly suggests that dysregulation of the Wnt/β-catenin pathway is involved in the tumorigenesis. β-catenin-mediated transcription is activated by the Wnt signaling pathway, which plays a crucial role in tumorigenesis. In the absence of Wnt signal, in the normal postembryogenesis period, the levels of β-catenin in cells are controlled by a multiprotein complex that includes adenomatous polyposis coli (APC) and glycogen synthase kinase-3β. Mutations in these components and mutations in *β-catenin* itself lead to excessive accumulation of β-catenin in the nucleus and aberrant stimulation of its target genes, which subsequently results in neoplasia.[17] This abnormal accumulation of β-catenin can be detected immunohistochemically.[13] Therefore, immunohistochemical staining for β-catenin has been used as a surrogate marker for the integrity of canonical Wnt signaling and β-catenin degradation.

In this study, we further performed mutational analyses of exon 3 of the *β-catenin* gene in ovarian MCSTs, because β-catenin-mediated signaling can be constitutively activated by truncation or mutation of serine and threonine residues in exon 3. As a result, we detected the same point mutation, c.98C > G, in exon 3 of *β-catenin* in both tumors. This mutation causes replacement of serine with cysteine at codon 33, leading to the loss of a phosphorylation site in the β-catenin protein. This Ser33 mutation is one of the major oncogenic *β-catenin* mutations that is more commonly detected in benign entities than in malignant tumors.[18] Therefore, we suggest that dysregulation of the Wnt/β-catenin pathway plays an important role in tumorigenesis of ovarian MCSTs. It is not yet clear whether all MCSTs harbor a specific S33C mutation in exon 3 of *β-catenin*. Some other cases may harbor mutations in different regions of this gene. It is also possible that alterations in the *APC* gene or in other genes involved in the Wnt/β-catenin pathway are involved in its tumorigenesis.

A discussion regarding the possible histologic differential diagnoses of ovarian MCSTs is necessary. First, the histology of MCSTs is so unique (ie, dissimilar to any other ovarian tumor) that after encountering a case or being aware of this disease entity there are hardly any other differential diagnoses. However, without knowledge of this entity, ovarian MCST can be confused morphologically with thecoma, AGCT/JGCT, YST, or SO. β-Catenin immunohistochemistry is useful for discriminating MCST from these tumors, because none of these tumors show nuclear β-catenin immunoreactivity. Other ovarian tumors such as sclerosing stromal tumors and steroid cell tumors may also be listed in the differential diagnoses, but not much is known regarding their β-catenin status.

The presence of thick fibrous stroma and growth of monotonous cells are common features observed in ovarian MCSTs and thecomas. However, significant differences are apparent between these 2 entities. Clinically, most thecomas occur in postmenopausal women,[3] and they frequently present with estrogenic symptoms.[23] In contrast, the majority of MCSTs are found in women aged 25 to 45 years. An estrogenic manifestation seems to be extremely rare in reported cases of MCSTs.[7] Macroscopically, thecomas are almost always solid and yellowish. Cystic changes or hemorrhagic changes that are frequently found in MCSTs are rarely observed in thecomas. There are differences in cellular features as well, particularly in the nuclear morphology. Cells with polygonal or spindle-shaped nuclei are far more prominent in thecomas than in MCSTs. Immunohistochemically, α-inhibin and calretinin, which are positive in most thecomas,[26] are negative in MCSTs. A variant of

thecoma, luteinized thecoma, often shows a microcystic growth pattern and may mimic MCST. However, luteinized thecomas are almost always bilateral and usually associated with sclerosing peritonitis. Immunohistochemically, luteinized thecomas do not show nuclear β-catenin accumulation. Luteinized cells in luteinized thecomas are positive for α-inhibin and calretinin.[22] Therefore, these markers should be useful for distinguishing an ovarian MCST from a luteinized thecoma.

There are certain similarities between MCSTs and AGCTs. AGCTs frequently exhibit a solid-cystic gross appearance, and hemorrhagic changes are occasionally seen. Monotonous growth of tumor cells is also common in MCSTs and AGCTs. However, significant differences are apparent in the histology between MCSTs and AGSTs. Tumor cells of MCSTs are predominantly round and lack nuclear grooves. In contrast, AGCT cells are short spindled, and they have characteristic nuclear grooves. In addition, microcystic/macrocystic structures of MCSTs differ from microfollicular/macrofollicular structures of AGCTs. In MCSTs, the tumor cells do not line up toward the cystic lumen. Structures such as Call-Exner bodies are absent in MCSTs. Recent studies have shown that a somatic mutation in the *FOXL2* gene (c.402C > G) is present in almost all (86 of 89, 97%) morphologically defined AGCTs.[2,8,10,20,21] In this study, we demonstrated the absence of this mutation in ovarian MCSTs. Hence, we expect that ovarian AGCTs and MCSTs also differ significantly in their genetic background. JGSTs tend to have cells with larger and more pleomorphic nuclei compared with MCSTs. Furthermore, mitotic figures are much more frequently found in JGSTs (median, 9.8/10 high-power fields).[19] In problematic cases, immunohistochemistry for α-inhibin and calretinin should be applied, because most AGCTs and JGCTs are positive for these markers.[19,26] Distinguishing an MCST from a sclerosing stromal tumor should not be too difficult, as microcysts are not a feature of sclerosing stromal tumors. Steroid cell tumors frequently have a hormonal presentation, and they typically show diffuse proliferation of tumor cells with an inconspicuous stroma. An intervening thick fibrous stroma, which is commonly seen in MCSTs, is usually absent in ovarian steroid cell tumors. As rare Sertoli-Leydig cell tumors have microcysts somewhat similar to those of MCSTs, thorough sampling of the tumor is recommended. Well-sampled Sertoli-Leydig cell tumors almost always reveal foci of typical Sertloi cell and Leydig cell growth. At low magnification, MCSTs can resemble YSTs, because both tumors show microcystic and/or reticular structures and frequent hemorrhagic changes. However, MCSTs do not show strong nuclear atypia that can be seen in YSTs. Immunohistochemistry for α-fetoprotein or SALL4 can help to distinguish between these tumors, because these markers are expressed by YSTs but not by MCSTs. SOs have a broad range of histology, and some may mimic MCSTs. In our experience, typical colloid that fills the follicles of SO is not observed in the cystic lumen of MCSTs. In difficult cases, we recommend performing immunohistochemistry for thyroid transcription factor-1, a known marker for thyroid tumors not expressed in MCSTs.

Finally, we mention ovarian SPN as a potential differential diagnosis for MCSTs. Deshpande et al[5] recently reported 3 cases of ovarian tumors that revealed similar morphologic and immunohistochemical features to pancreatic SPN and proposed the entity "solid pseudopapillary tumor of the ovary." In our observations, morphologic features of MCST and SPN were similar in some aspects. Growth of round-to-spindled monotonous cells was common in both tumors, and solid areas of growth in MCSTs and SPNs closely resembled each other. However, certain differences were also apparent. Pseudopapillary structure, which is characteristic of SPNs, was absent in MCSTs. Immunoreactivity for markers such as WT-1, CD56, and progesterone receptor also differed between SPNs and MCSTs. Interestingly, in the report by Deshpande et al,[5] β-catenin nuclear immunoreactivity was observed in all 3 ovarian SPN cases. Although a mutation analysis was not performed in their study, dysregulation of Wnt/β-catenin signaling could theoretically be involved in the development of ovarian SPNs. Their results and our results suggest a possible link between ovarian SPNs and MCSTs. We hope to further examine similarities and differences between ovarian MCSTs and SPNs in the future on the basis of a larger number of cases.

In conclusion, we presented the distinct features of ovarian MCST from morphologic, immunohistochemical, and genetic viewpoints. Dysregulation of Wnt/β-catenin signaling is involved in the pathogenesis of ovarian MCST. The findings presented here provide insight into this unique entity and will facilitate future studies.

ACKNOWLEDGMENT

The authors thank Yumiko Nagano for her tremendous technical support.

REFERENCES

1. Abraham SC, Klimstra DS, Wilentz RE, et al. Solid-pseudopapillary tumors of the pancreas are genetically distinct from pancreatic ductal adenocarcinomas and almost always harbor beta-catenin mutations. *Am J Pathol.* 2002;160:1361–1369.
2. Benayoun BA, Caburet S, Dipietromaria A, et al. Functional exploration of the adult ovarian granulosa cell tumor-associated somatic FOXL2 mutation p.Cys134Trp (c.402C > G). *PLoS One.* 2010;5:e8789.
3. Björkholm E, Silfverswärd C. Theca-cell tumors: clinical features and prognosis. *Acta Radiol Oncol.* 1980;19:241–244.
4. Dabbs DJ, Sturtz K, Zaino RJ. The immunohistochemical discrimination of endometrioid adenocarcinomas. *Hum Pathol.* 1996;27:172–177.
5. Deshpande V, Oliva E, Young RH. Solid pseudopapillary neoplasm of the ovary: a report of 3 primary ovarian tumors resembling those of the pancreas. *Am J Surg Pathol.* 2010;34:1514–1520.
6. Eichhorn JH, Young RH, Clement PB. Sertoliform endometrial adenocarcinoma: a study of four cases. *Int J Gynecol Pathol.* 1996;15:119–126.
7. Irving JA, Young RH. Microcystic stromal tumor of the ovary: report of 16 cases of a hitherto uncharacterized distinctive ovarian neoplasm. *Am J Surg Pathol.* 2009;33:367–375.

8. Jamieson S, Butzow R, Andersson N, et al. The FOXL2 C134W mutation is characteristic of adult granulosa cell tumors of the ovary. *Mod Pathol.* 2010;23:1477–1485.
9. Kandalaft PL, Esteban JM. Bilateral massive ovarian leiomyomata in a young woman: a case report with review of the literature. *Mod Pathol.* 1992;5:586–589.
10. Kim MS, Hur SY, Yoo NJ, et al. Mutational analysis of FOXL2 codon 134 in granulosa cell tumour of ovary and other human cancers. *J Pathol.* 2010;221:147–152.
11. Köbel M, Gilks CB, Huntsman DG. Adult-type granulosa cell tumors and FOXL2 mutation. *Cancer Res.* 2009;69:9160–9162.
12. Maeda D, Takazawa Y, Oda K, et al. Glomus tumor of the ovary: a case report. *Int J Surg Pathol.* 2010;18:557–560.
13. Ng TL, Gown AM, Barry TS, et al. Nuclear beta-catenin in mesenchymal tumors. *Mod Pathol.* 2005;18:68–74.
14. Notohara K, Hamazaki S, Tsukayama C, et al. Solid-pseudopapillary tumor of the pancreas: immunohistochemical localization of neuroendocrine markers and CD10. *Am J Surg Pathol.* 2000;24:1361–1371.
15. Oliva E, Garcia-Miralles N, Vu Q, et al. CD10 expression in pure stromal and sex cord-stromal tumors of the ovary: an immunohistochemical analysis of 101 cases. *Int J Gynecol Pathol.* 2007;26:359–367.
16. Otis CN, Powell JL, Barbuto D, et al. Intermediate filamentous proteins in adult granulosa cell tumors: an immunohistochemical study of 25 cases. *Am J Surg Pathol.* 1992;16:962–968.
17. Polakis P. Wnt signaling and cancer. *Genes Dev.* 2000;14:1837–1851.
18. Provost E, Yamamoto Y, Lizardi I, et al. Functional correlates of mutations in beta-catenin exon 3 phosphorylation sites. *J Biol Chem.* 2003;278:31781–31789.
19. Schneider DT, Jänig U, Calaminus G, et al. Ovarian sex cord-stromal tumors: a clinicopathological study of 72 cases from the Kiel Pediatric Tumor Registry. *Virchows Arch.* 2003;443:549–560.
20. Schrader KA, Gorbatcheva B, Senz J, et al. The specificity of the FOXL2 c.402C > G somatic mutation: a survey of solid tumors. *PLoS One.* 2009;4:e7988.
21. Shah SP, Köbel M, Senz J, et al. Mutation of FOXL2 in granulosa-cell tumors of the ovary. *N Engl J Med.* 2009;360:2719–2729.
22. Staats PN, McCluggage WG, Clement PB, et al. Luteinized thecomas (thecomatosis) of the type typically associated with sclerosing peritonitis: a clinical, histopathologic, and immunohistochemical analysis of 27 cases. *Am J Surg Pathol.* 2008;32:1273–1290.
23. Stage AH, Grafton WD. Thecomas and granulosa-theca cell tumors of the ovary: an analysis of 51 tumors. *Obstet Gynecol.* 1977;50:21–27.
24. Tanaka Y, Kato K, Notohara K, et al. Frequent beta-catenin mutation and cytoplasmic/nuclear accumulation in pancreatic solid-pseudopapillary neoplasm. *Cancer Res.* 2001;61:8401–8404.
25. Tiltman AJ, Haffajee Z. Sclerosing stromal tumors, thecomas, and fibromas of the ovary: an immunohistochemical profile. *Int J Gynecol Pathol.* 1999;18:254–258.
26. Zhao C, Vinh TN, McManus K, et al. Identification of the most sensitive and robust immunohistochemical markers in different categories of ovarian sex cord-stromal tumors. *Am J Surg Pathol.* 2009;33:354–366.

Cancer Gene Therapy (2011) 18, 587–597

www.nature.com/cgt

ORIGINAL ARTICLE

Enhanced specificity of HPV16 E6E7 siRNA by RNA–DNA chimera modification

K Yamato[1], N Egawa[2], S Endo[3], K Ui-Tei[4], T Yamada[5], K Saigo[4], I Hyodo[3], T Kiyono[2] and I Nakagawa[1]

[1]*Section of Bacterial Pathogenesis, Graduate School of Medical and Dental Science, Tokyo Medical and Dental University, Tokyo, Japan;* [2]*Division of Virology, National Cancer Center Research Institute Tokyo, Tokyo, Japan;* [3]*Department of Gastroenterology, Institute of Clinical Medicine, University of Tsukuba Ibaraki, Ibaraki, Japan;* [4]*Department of Biophysics and Biochemistry, Graduate School of Science, University of Tokyo, Tokyo, Japan and* [5]*Division of Pathology, Keio University, School of Medicine, Tokyo, Japan*

Although efforts have been made to develop new drugs for infectious and neoplastic diseases utilizing synthetic small interfering RNA(siRNAs), those intrinsically have undesirable effects, including silencing of unintended genes (off-target effect) and nonspecific cytotoxicity. Off-target effects can be avoided by DNA substitution in the guide strand (GS) seed region of nucleotide positions 1–8 and its complementary part of the passenger strand plus the 3′ overhang, which is designated as a double-strand RNA–DNA chimera (dsRDC). In this study, we found that the specificity of potent siRNAs targeting human papillomavirus 16 (HPV16) E6 and E7 oncogenes, which we previously reported, could be enhanced by short dsRDC modification (first six nucleotides from the 5′ end of the GS and its complementary nucleotides of the passenger strand). Such dsRDC modification reduced nonspecific cytotoxicity in two of three siRNAs (497 and 752), although not in the other (573), which correlated with their off-target effects. In addition, silencing activity was marginally impaired in two dsRDCs (497 and 573) and moderately in one (752). Finally, dsRDC-497 induced E6E7-specific growth suppression of cervical cancer cells as well as E6E7-immortalized human keratinocytes. Our results show that dsRDC modification enhances the specificity of E6E7 siRNA, which is required for use in *in vivo* settings.
Cancer Gene Therapy (2011) **18,** 587–597; doi:10.1038/cgt.2011.28; published online 10 June 2011

Keywords: siRNA therapy; HPV16; cervical cancer; off-target effect

Introduction

A decade has passed since the discovery of RNA interference (RNAi) induction by synthetic 21–23-nucleotide double-stranded small interfering RNA (siRNA) in mammalian cells.[1,2] Since then, siRNA has become a powerful tool for studying gene functions, as well as development of potential drugs for viral infections and cancer treatments. However, the effects of siRNA are not as specific as initially proposed. siRNA silences the expression of unintended targets with partial sequence complementarities (off-target effects),[3,4] although minimal matching of mRNA and the seed region of the siRNA guide strand (GS) (nucleotide positions 2–8 from the 5′ end) may be sufficient for off-target silencing.[3,5,6] Nucleotide modifications at specific positions have been found to overcome the off-target problem.[7–9] In addition, DNA replacement in the seed region of the GS (positions 1–8 from the 5′ end) and its complementary sequence of the passenger strand (PS), designated as double-stranded RNA–DNA chimera (dsRDC), abolishes the off-target effects with some decrease in silencing activity.[8] Most active siRNAs have been shown to induce a cytotoxic effect by exerting off-target silencing and interfering with the endogenous RNAi pathway,[7,9–12] whereas cytotoxicity might be reduced by use of chemically modified siRNA with low off-target activity[7] or siRNA with high silencing activity at a minimal concentration.

Cervical cancer is the second most common female malignancy throughout the world, with high-risk types of human papillomavirus, such as types 16, 18, 33, 45 and 31, known to be causative agents.[13] Among them, HPV16 is the most prevalent and accounts for about half of reported cases. High-risk types of human papillomaviruses are small DNA viruses with a circular double-stranded DNA genome of about 8000 base pairs (bp) containing an upstream regulatory region, along with six early (E6, E7, E1, E2, E4 and E5) and two late (L1 and L2) genes. High-risk types of human papillomaviruses exert carcinogenic effects through constitutive expressions

Correspondence: Dr K Yamato, Section of Bacterial Pathogenesis, Graduate School of Medical and Dental Science, Tokyo Medical and Dental University, 1-5-45 Yushima, Bunkyo-kyu, Tokyo 113-8549, Japan.
E-mail: yamato.bac@tmd.ac.jp
Received 28 December 2010; revised 2 March 2011; accepted 30 April 2011; published online 10 June 2011

of the E6 and E7 oncogenes.[14–17] Uncontrolled expressions of E6 and E7, which are functionally equivalent to *P53* and *RB* mutations in other cancer types, also contribute to cellular immortalization, genetic instability, accumulation of additional genetic changes and resultant malignant transformation. In addition, their expressions are essential for maintaining a malignant phenotype, whereas their suppression results in apoptosis and cellular senescence by restoring and activating the functions of *P53* and *RB*.[18–24] Thus, E6 and E7 are considered to be ideal therapeutic targets. Prophylactic vaccines covering HPV16 and 18 are now clinically available, and have been shown effective for preventing infections as well as cervical cancer.[25] However, these vaccines do not benefit individuals who are already infected and their long-term effects remain to be confirmed. Thus, it is necessary to develop new therapies for patients who have persistent infections, precancerous lesions or overt cancer.

A large number of siRNA sequences targeting HPV16 E6E7 oncogenes have been found to exert negative growth effects on HPV16-positive cancer cells.[21–23,26] Among them, we previously reported that three siRNAs (497, 573 and 752) were highly potent.[27] In this study, we investigated the effects of short dsRDC modification (positions 1–6 from the 5′ end of the GS and its complementary parts of the PS) on cytotoxicity and off-target effects exerted by some of those potent E6E7 siRNAs. We found that most of the nonspecific cytotoxicity was attenuated by dsRDC modification with a concomitant marginal or moderate reduction in silencing activity. Among those modified dsRDCs, one with high target specificity and preserved silencing activity suppressed the growth of E6E7-immortalized human keratinocytes, an early cancer model, as well as cervical cancer cells. These findings indicate the potential of E6E7 dsRDC in therapeutic applications for HPV16-related diseases.

Materials and methods

Cell lines and plasmid transfection

SiHa (HPV16-positive cervical cancer), HeLa (HPV16-negative cervical cancer) and SNU-1 (gastric cancer) cell lines were purchased from American Type Culture Collection (ATCC, Rockville, MD). SiHa and HeLa cells were cultured in Dulbecco's modified Eagle's medium containing 10% heat-inactivated fetal calf serum. SNU-1 cell lines were cultured in RPMI1640 medium containing 10% fetal calf serum. Primary human keratinocytes (HDK) were purchased from Cell Applications (San Diego, CA) and immortalized by the catalytic subunit of *human TERT* basically, as described previously,[28] except that the present HDK were transduced with *human TERT* alone, and not a combination of *human TERT* and *Bmi-1* (HDK1-T). Generation of HPV16 E6E7-immortalized HDK (HDK1-E6E7) was performed as reported previously.[28] HDK, HDK1-T and HDK1-E6E7 were cultured in serum-free keratinocyte media with recombinant epidermal growth factor (5 ng ml^{-1}) and bovine pituitary extract (5 μg ml^{-1}) (Invitrogen, Carlsbad, CA) at 37 °C in an atmosphere of 5% CO_2. Generation of stable clones expressing firefly luciferase (FLuc) (FL-SiHa-2, FL-HeLa-1) was as reported previously.[27] Plasmid transfection was performed using Lipofectamine 2000 transfection reagent (Invitrogen) according to the manufacturer's instructions.

siRNAs and transfection

The sequences of the siRNAs used in this study[27] are summarized in Supplementary Table 1. All siRNAs were designed using the siDirect software (http://sidirect2.rnai.jp/), as reported previously.[29] Control siRNA was an artificial sequence designed to have the least homology to human and mouse genes. Control siRNA and its dsRDC-modified form were included in all experiments. For preparation of dsRDCs, six nucleotides from the 5′ end of GS and eight from the 3′ end of PS were substituted with corresponding DNAs. Twenty-one-base nucleotides were synthesized, 2′-deprotected, desalted and annealed in buffer (100 mM potassium acetate, 30 mM HEPES-KOH at pH 7.4, 2 mM magnesium acetate).

At 1 day before transfection, cells were plated at a density of 2–4 × 10^4 cells per well in 24-well plates containing 0.5 ml of Dulbecco's modified Eagle's medium with 10% fetal calf serum. For analysis of the effects of siRNA on cell growth and viability, cells were plated at a low density (1–2 × 10^3 cells per well) in 96-well plates containing 0.1 ml of Dulbecco's modified Eagle's medium containing 10% fetal calf serum. Various amounts of siRNA and Lipofectamine RNAiMAX (0.6 μl) (Invitrogen), both of which were added along with Opti-MEM I reduced serum medium (Opti-MEM, Invitrogen) up to 50 μl, were combined, incubated at room temperature for 20 min and then added to 0.5-ml cultures. For transfection of SiHa cells and their derivatives, 1 μl of Lipofectamine RNAiMAX was used. For transfection of immortalized keratinocytes, the culture medium was replaced at 5 h after transfection. For co-transfection of HeLa cells with the plasmid and siRNA or dsRDC, Lipofectamine 2000 was used.

Plasmid construction

Renilla luciferase (RLuc) cDNA fused with HPV16 E6 (231–559) (RLuc-ΔNE6) and RLuc-E7 (562–858) were isolated from 16ΔNE6/psiCheck-2 and 16E7/psiCheck-2,[27] respectively, and then cloned into pZeoSV2 (Invitrogen) at the *Nhe*I and *Not*I sites. The resultant plasmids were designated as 16ΔNE6/pZeoSV2 and 16E7/pZeoSV2, respectively. Construction of RLuc-ΔNE6E7/psiCheck-2 was reported previously.[27] Next, 19-nucleotide human gene sequences carrying 3-nucleotide mismatches to GS of each E6E7 siRNA were selected using the siDirect software[29] (Table 1). The sense and antisense oligoDNAs of these sequences are summarized in Supplementary Table 2. Sense and antisense oligoDNAs were phosphorylated, annealed and subcloned at the *Xho*I and *Not*I sites of psiCheck-2 (Promega, Madison, WI).

Table 1 Off-target candidate human genes carrying 3-nucleotide mismatches to GS of siRNAs targeting HPV16 E6E7

Sequence name	*OT gene accession number*	*Gene definition and gene symbol*	*GS sequence (3′←5′)* *OT mRNA (5′→3′)*
497OT-1	BX647877	cDNA clone DKFZp313E2325	GAUCUGUCGAUGUAUGUUU ||X|X||||||||||X| CUGGCCAGCUACAUACAGA
497OT-2	NM_006237.2	*POU4F1*	UACCUGUCCAUGUAUGUCU X|||X|||X||||||||| CUGGCCAGCUACAUACAGA
573OT-1	NM_000922.2	*PDE3B*	CACAUACAUUGAAUAAAUA |||X||||||X||X|||| GUGGAUGUAACGUACUUAU
573OT-2[a]	AL832149	cDNA clone DKFZp686P15111	CACCUACACAGCAUGAAUU ||||||||XX|||||||X GUGGAUGUAACGUACUUAU
573OT-3	NM_001517.4	*GTF2H4*	CACCUACAAUGCAGGAAUC ||||||||X||||X||||X GUGGAUGUAACGUACUUAU
573OT-4[a]	BF693154	cDNA clone IMAGE:4244422 5′	CACCUACACAGCAUGAAUU ||||||||XX|||||||X GUGGAUGUAACGUACUUAU
573OT-5[b]	AF138859	cDNA clone FLB2932	CAACUACAUUACAUUAAUA ||X|||||||X|||X|||| GUGGAUGUAACGUACUUAU
573OT-6[b]	BC036590	cDNA clone IMAGE:4801089	CAACUACAUUACAUUAAUA ||X|||||||X|||X|||| GUGGAUGUAACGUACUUAU
573OT-7	NM_004582.2	*RABGGTB*	CAACUUCAUCGCAUGAAUA ||X||X|||X||||||||| GUGGAUGUAACGUACUUAU
573OT-8	AA861522	cDNA clone IMAGE:1407653 3′	CUCCUACAUUGUAGGAAUA |X||||||||X|X|||| GUGGAUGUAACGUACUUAU
573OT-9	F03276	cDNA clone c-1sa08 3′	CACCUCCAUUUAAUGAAUA |||||X||||XX||||||| GUGGAUGUAACGUACUUAU
752OT-1	BQ054887	cDNA clone IMAGE:5806941 5′	CUUCGGCUGCGCGUAAAAA ||||||X||X|||||X||| GAAGCCAACACGCAUGUUU

Abbreviations: GS, guide strand; HPV, human papillomavirus; OT, off-target candidate; PS, passenger strand; siRNA, small interfering RNA.

All human genes with 3-nucleotide mismatches to the GS of each E6E7 siRNA were selected using the siDirect software.

Matched and mismatched base pairs between off-target candidate sequences and GSs are visualized by vertical lines and cross marks, respectively.

[a]The sequence of 573OT-4 is identical to that of 573OT-2.

[b]The sequence of 573OT-6 is identical to that of 573OT-5.

Immortalized human keratinocytes stably expressing FLuc

FLuc cDNA was amplified using a polymerase chain reaction (PCR) method with Platinum PCR Supermix High Fidelity (Invitrogen) and sense and antisense primers, with psiCheck2 utilized as a template. The PCR product was cloned into pCR8/GW/TOPO (Invitrogen) using Topoisomerase I (Invitrogen) and sequenced (FLuc/pCR8/GW). FLuc cDNA was then subcloned in a lentivirus expression plasmid (pLenti6.3/V5-DEST; Invitrogen) with LR Clonase II (Invitrogen) and the resultant lentivirus plasmids were designated as FLuc/pLenti6.3. An infectious recombinant virus was produced by co-transfection of 293FT cells (Invitrogen) with FLuc/pLenti6.3 and packaging plasmids (pLP1, pLP2 and pLP/VSVG) (Invitrogen) using Lipofectamine 2000, according to the manufacturer's instructions. The culture medium was changed at 24 h and collected at 96 h after transfection. HDK1-T and HDK1-E6E7 were infected with a recombinant lentivirus for 6 h in the presence of polybren (6 $\mu g\,ml^{-1}$), and then selected using 2.5 $\mu g\,ml^{-1}$ of blasticidin (Invitrogen), and FLuc-expressing cells were designated as HDK1-T-luc and HDK1-E6E7-luc, respectively.

SiHa cells stably expressing FLuc and RLuc-E6, or RLuc-E7, and luciferase assay

SiHa cells stably expressing both FLuc and RLuc-E6 (RL-E6-FL-SiHa-10), and those expressing both FLuc and RLuc-E7 (RL-E7-FL-SiHa-2) were obtained by

transfection of FL-SiHa-2 cells[27] with 16ΔNE6/pZeoSV2 and 16E7/pZeoSV2, respectively, and antibiotic selection using both zeocin (1 mg ml^{-1}; Invitrogen) and G418 (1 mg ml^{-1}; Invitrogen). For luciferase assays, cells were harvested at 48 h after transfection with siRNA or dsRDC, and then luciferase activity was determined using a Dual Luciferase Reporter Assay System (Promega).

Real-time quantitative reverse transcription-PCR

Total RNA was extracted from cells using a High Pure RNA Isolation Kit (Roche Diagnostics, Mannheim, Germany), according to the manufacturer's instructions. cDNA was synthesized using a Transcriptor First Strand cDNA Synthesis Kit (Roche Diagnostics). Real-time quantitative reverse transcription-PCR assays were performed using a LightCycler 480 System (Roche Diagnostics) in 96-well plates. Each reaction was carried out in 20 μl containing 10 μl of LightCycler 480 Probes Master (Roche Diagnostics), 5 μl of cDNA from a 10 × dilution of the reverse transcriptase reaction (equivalent to 25 ng of reverse-transcribed RNA), 900 nM of a forward and reverse prime pair and 250 nM of 6-carboxyfluorescein-labeled probe. Serial dilutions of plasmid DNA (10–0.01 ng) were used to generate a standard curve. The LightCycler protocol was used as follows: initial cycle of 95 °C for 10 min, followed by 40 cycles of 95 °C for 15 s and 60 °C for 1 min. Water was used as the template for negative control amplifications included with each PCR run. All reactions were performed in triplicate in each 96-well plate. Data were analyzed using the Roche LightCycler 480 software and the crossing point (Cp) value was calculated with the Second Derivative Maximum Method. The amount of target mRNA was examined and normalized to that of 18S ribosomal RNA.

The primers and probes for E6-E7 and E6*I-E7 have been described by others.[30] Those for 18S ribosomal RNA and AL832149 were designed by Sigma Aldrich Japan (Tokyo, Japan) and Applied Biosystems (Foster City, CA), respectively. Primers and probes for *POU4F1* (NM_006237.3) and *GTF2H4* (NM_001517.4) were obtained from Applied Biosystems (*POU4F1*, Assay ID Hs00366711_m1; *GTF2H4*, Assay ID Hs00231008_m1). All probes were labeled at the 5′ end with the reporter dye 6-carboxyfluorescein and at the 3′ end with a non-fluorescent quencher. The PCR primer and probe sequences are listed in Supplementary Table 3.

Analysis of cell growth and senescence-associated β-galactosidase staining

Cell viability was examined with a colorimetric assay using WST-8 (Cell Counting Kit 8; Dojin Laboratories, Kumamoto, Japan), according to the manufacturer's instructions. Senescence-associated β-galactosidase (SAβ-gal) staining was performed using a Senescent Cell Staining Kit (Sigma-Aldrich). The viability of HDK1-T-luc and HDK1-E6E7-luc cells was determined using a Luciferase Assay System (Promega).

Statistical analysis

The statistical significance of differences was determined using an unpaired two-tailed Student's *t*-test. Differences were considered statistically significant at $P<0.05$.

Results

Silencing activities of E6E7 siRNAs and their dsRDC counterparts

In this study, we examined whether dsRDC modification of HPV16 E6E7 siRNAs with high silencing activity (497, 573 and 752; Figure 1a) would increase their target specificity and reduce nonspecific cytotoxicity. dsRDCs with an 8-nucleotide DNA substitution often show lower silencing activity than those with a 6-nucleotide DNA substitution (data not shown). We used the shorter DNA substitution in this study (Figure 1b).

HPV16 E6E7 siRNAs (497, 573 and 752) and their dsRDC forms were compared with regard to their silencing activity using HeLa cells transiently expressing RLuc-E6E7. HeLa cells were co-transfected with RLuc-E6E7-expressing plasmids along with siRNAs (control, 497, 573 and 752) and their dsRDC counterparts. At 48 h after transfection, a dual luciferase assay was performed. As shown in Figure 1c, siRNAs 497, 573 and 752 exhibited potent silencing activity (8.4, 11.6 and 5.6%, respectively), whereas control siRNA showed very mild suppression (72.1%). dsRDC modification of these siRNAs slightly reduced the silencing activities of siRNAs 497 and 573 (16.2 and 13.6%), and moderately that of 752 (22.0%). SiHa cells stably expressing both RLuc-E6 and FLuc (RL-E6-FL-SiHa-10) were used for determining the half-maximal inhibitory concentration (IC_{50}) values of siRNA-497 and its dsRDC. Various concentrations of siRNA and dsRDC were transfected into RL-E6-FL-SiHa-10 cells, and then a dual luciferase assay was performed 48 h after transfection. siRNA-497 showed maximal suppression of RLuc activity to 4.6% at 5 nM with an IC_{50} of 0.015 nM, whereas dsRDC modification slightly decreased the silencing activity by 6.8-fold (IC_{50}, 0.105 nM) (Figure 1d). Similarly, siRNAs targeting E7 (573 and 752) were analyzed with RL-E7-FL-SiHa-2 cells expressing RLuc-E7 and FLuc. siRNA-573 had a high silencing activity with an IC_{50} of 0.019 nM and dsRDC modification increased the IC_{50} by 5.2-fold (0.098 nM; Figure 1e). In contrast to the other two dsRDCs, dsRDC-752 had a low level of silencing activity and was 32-fold less active than its siRNA form (IC_{50} 1.774 vs 0.055 nM) (Figure 1f). Both control siRNA and dsRDC had negligible effects at 1 nM on RLuc expression in RL-E6-FL-SiHa-10 and RL-E7-FL-SiHa-2 cells (data not shown).

Effects of E6E7 dsRDC on endogenous E6E7 mRNAs

The effects of dsRDCs targeting E6E7 on endogenous E6-E7 and E6*I-E7 mRNA expressions were compared with their siRNA counterparts using HPV16-positve cervical cancer cells. FL-SiHa-2 cells were transfected with siRNAs (control, 497, 573 and 752) or their dsRDC

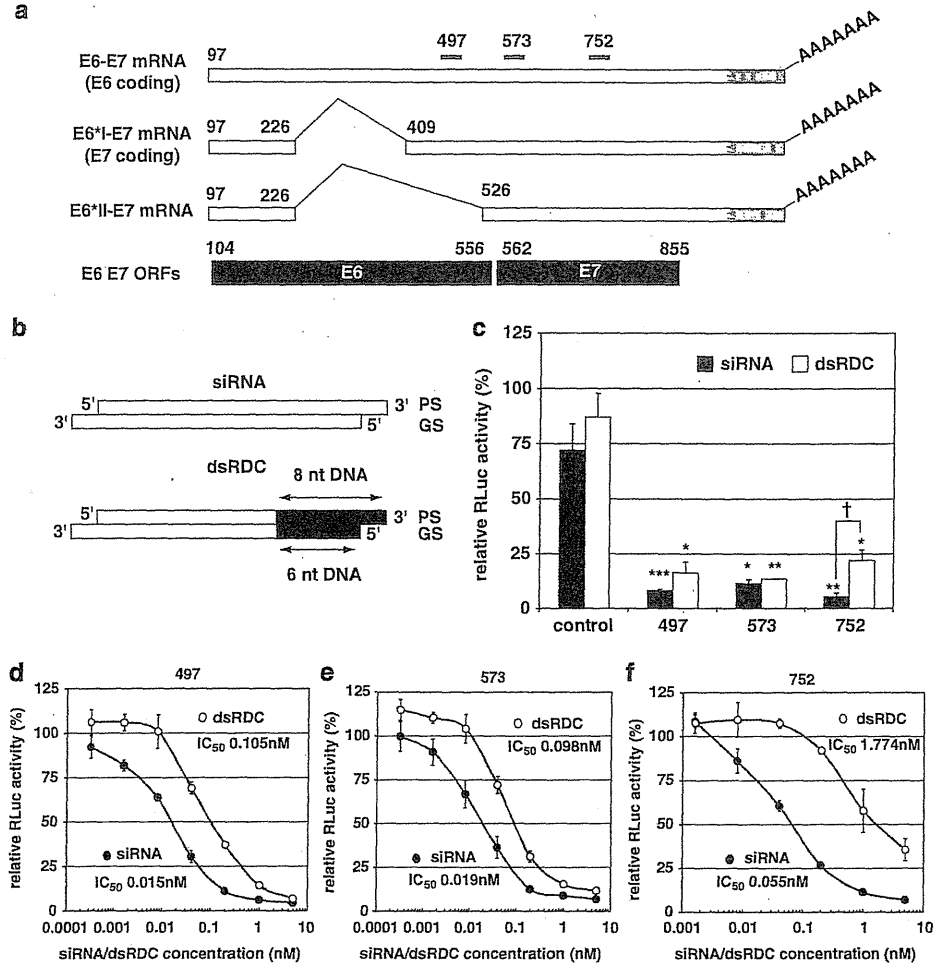

Figure 1 RNA–DNA chimera modification of small interfering RNA (siRNA) targeting human papillomavirus 16 (HPV16) E6E7. (**a**) E6E7 mRNA and splicing variants, and E6E7 siRNAs. siRNAs targeting E6 and E7 are depicted as short lines (top). Open bars represent mRNAs coding E6 and E7 with introns within E6 (middle). Gray area indicates cellular sequence derived from the chromosomal integration site. Closed boxes show locations of the E6 and E7 coding regions of the HPV16 prototype (accession number K02718) (bottom). Numbers refer to the locations of the transcription initiating site and splicing junctions. ORF, open reading frame. (**b**) Structure of double-strand RNA–DNA chimera (dsRDC). Conventional siRNA is a 19-bp long double-stranded RNA with 2-nucleotide 3′ overhangs. The dsRDCs used in this study contained 6-nucleotide DNA in the 5′ region of the guide strand and 8-nucleotide DNA in the 3′ region of the PS. Open and closed bars represent ribonucleic acid and deoxyribonucleic acid, respectively. PS, passenger strand; GS, guide strand. Silencing activities of control and HPV16 E6E7 targeting siRNAs (497, 573 and 752), and their dsRDC forms were determined by transient transfection of HeLa cells with a *Renilla* luciferase (RLuc)-E6E7/psiCheck-2 plasmid, as well as siRNAs and dsRDCs. At 48 h after transfection, a dual luciferase assay was performed. RLuc activities are shown as relative to mock-transfected cells (**c**). The half-maximal inhibitory concentration (IC_{50}) values of siRNA and dsRDC targeting E6 (497) were determined using SiHa cells stably expressing firefly luciferase (FLuc) and artificial fusion mRNA of RLuc-E6 (RL-E6-FL-SiHa-10) (**d**), whereas those targeting E7 (573 and 752) were analyzed using SiHa cells stably expressing FLuc and RLuc-E7 (RL-E7-FL-SiHa-2) (**e**, **f**). Cells were transfected with various concentrations of siRNAs or dsRDCs, and then analyzed using a dual luciferase assay 48 h after transfection. RLuc activities were normalized to those of FLuc. RLuc activities are shown as relative to mock-transfected cells. Experiments were performed in triplicate and error bars represent the standard deviation from the mean. Data points marked with asterisks are statistically significant as compared with control transfection (*$P<0.001$; **$P<0.01$; ***$P<0.05$). Data points marked with crosses are statistically significant ($^{\dagger}P<0.01$).

counterparts at 5 nM for 72 h, and then analyzed for levels of mRNAs coding E6 and E7 by quantitative reverse transcription-PCR. As shown in Table 2, transfection with siRNAs 497, 573 and 752 decreased the levels of both E6-E7 and E6*I-E7 mRNA to 13.5–27.6 and 3.2–6.4%, respectively. Their dsRDC counterparts 573 and 752 were less active, although they still suppressed those levels to 30.9–32.7 and 17.2–31.2%, respectively. dsRDC-497 also suppressed E6*I-E7 mRNA expression to 24.9%, however, its effect on E6-E7 mRNA expression was indistinguishable from that of control dsRDC (64.7 vs 67.2%). Thus, dsRDC modification of most E6E7 siRNAs slightly decreased the silencing activity towards E6-E7 and E6*I-E7 mRNA expressions, except for dsRDC-497, which exerted a silencing effect only on E6*I-E7 mRNA and not on E6-E7 mRNA.

Effects of HPV16 E6E7 siRNAs and dsRDCs on growth of HPV16-positive and -negative cancer cells

To examine if dsRDCs targeting E6E7 are capable of inducing specific growth inhibition of HPV16-related cancer cells, the effects of dsRDC on cell growth were examined using HPV16-positive (FL-SiHa-2) and -negative cells (FL-HeLa-1). Control and E6E7 dsRDCs (497, 573 and 752) as well as their siRNA counterparts were transfected into FL-SiHa-2 cells at 2 nM. All E6E7 dsRDCs tested in this study suppressed the growth of FL-SiHa-2 cells, although the effects of two of the dsRDCs (497 and 752) were less potent as compared with those of their siRNA counterparts (Figure 2a).

HeLa and FL-HeLa-1 cells are highly vulnerable to siRNA-mediated nonspecific cytotoxicity.[9,27] By taking advantage of this characteristic, E6E7 dsRDC and siRNA (497, 573 and 752) were evaluated for their nonspecific cytotoxicity by determining cell viability 7 days after transfection. As shown in Figure 2b, all siRNAs including the control showed moderate to strong growth suppression toward FL-HeLa-1 cells. dsRDC modification of these siRNAs (control, 497 and 752), except for 573, also decreased cytotoxicity as compared with their siRNA counterparts. These results suggest that most siRNAs induce nonspecific cytotoxicity[9] and that dsRDC modification reduces the level of cytotoxicity.

The negative growth effect of E6E7 siRNA on E6E7-positive cancer cells is mediated in part by inducing cellular senescence.[24,26,27] We examined if E6E7 dsRDCs capable of specific growth suppression (497 and 752) also induced senescence in FL-SiHa-2 cells. siRNA-573 and its dsRDC were omitted, because of their strong nonspecific toxicity. Cells were transfected with either control siRNA, E6E7 siRNA or their dsRDC counterparts for 7 days, and then tested for the expression of SAβ-gal, a hallmark of cellular senescence. The proportions of SAβ-gal-positive cells transfected with control siRNA and dsRDC was 8.6 and 3.5%, respectively, whereas those of siRNA-497- and dsRDC-497-induced cells were 64.1 and 70.3%, respectively. dsRDC-752 induced a slightly lower percentage of SAβ-gal-positive cells (46.6%) than its siRNA counterpart (78.8%) (Figure 2c). Thus, it was shown that E6E7 dsRDC exerts growth suppression in HPV16-positive cancer cells through a mechanism similar to that of siRNA.

Table 2 qRT-PCR analysis of E6-E7 and E6*I-E7 mRNA levels in FL-SiHa-2 cells transfected with siRNAs and dsRDCs targeting HPV16 E6E7

siRNA/dsRDC	*E6-E7 mRNA (%)*	*E6*I-E7 mRNA (%)*
Mock	100.0 ± 5.0	100.0 ± 10.8
Control		
siRNA	53.8 ± 4.1	55.3 ± 8.1
dsRDC	67.2 ± 1.3	72.2 ± 3.6
497		
siRNA	27.6 ± 0.7	5.9 ± 0.6
dsRDC	64.9 ± 4.2	24.9 ± 1.9
573		
siRNA	21.4 ± 1.1	6.4 ± 0.7
dsRDC	30.9 ± 0.9	17.2 ± 0.9
752		
siRNA	13.5 ± 1.1	3.2 ± 0.4
dsRDC	32.7 ± 0.9	31.2 ± 2.9

Abbreviations: dsRDC, double-strand RNA–DNA chimera; FL, firefly luciferase; HPV, human papillomavirus; qRT-PCR, quantitative reverse transcription-polymerase chain reaction; s.d., standard deviations; siRNA, small interfering RNA.

E6-E7 and E6*I-E7 mRNA levels were analyzed by qRT-PCR and were normalized to that of 18S rRNA. Mean values and s.d. of relative mRNA levels (%) to mock-transfected cells are shown. Experiments were carried out in triplicate.

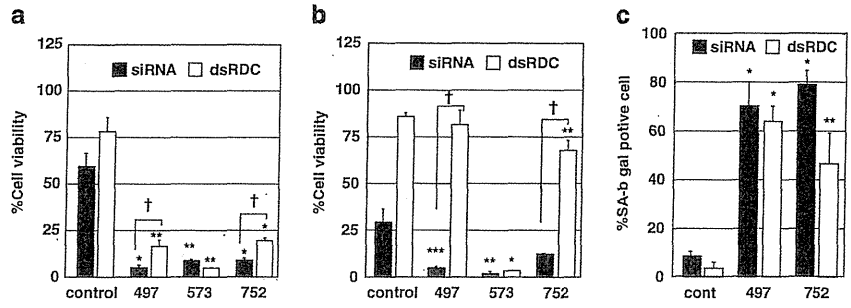

Figure 2 Effects of E6E7 double-strand RNA–DNA chimera (dsRDCs) on growth of human papillomavirus 16 (HPV16)-positive and -negative cervical cancer cells. HPV16-positive FL-SiHa-2 (**a**) and HPV16-negative (FL-HeLa-1) cells (**b**) were transfected with either mock, small interfering RNA (siRNA) (control, 497, 573 and 752) or their dsRDC counterparts at 2 nM. Cell viability was determined using a WST-8 assay 5–7 days after transfection. Cell viability relative to the mock-transfected cells is shown. (**c**) Induction of senescence-associated β-galactosidase (SAβ-gal) activity in FL-SiHa-2 cells by dsRDCs targeting E6E7. FL-SiHa-2 cells were transfected with mock, siRNA (control, 497 and 752) (1 nM) or dsRDC (control, 497 and 752) (2 nM) for 7 days, and then stained for SAβ-gal activity. Values for SAβ-gal-positive cells are shown as percentages. All assays were performed in triplicate and error bars represent the standard deviation from the mean. Data points marked with asterisks are statistically significant as compared with control transfection (*$P<0.001$; **$P<0.01$; ***$P<0.05$). Data points marked with crosses are statistically significant ($^{\dagger}P<0.01$).

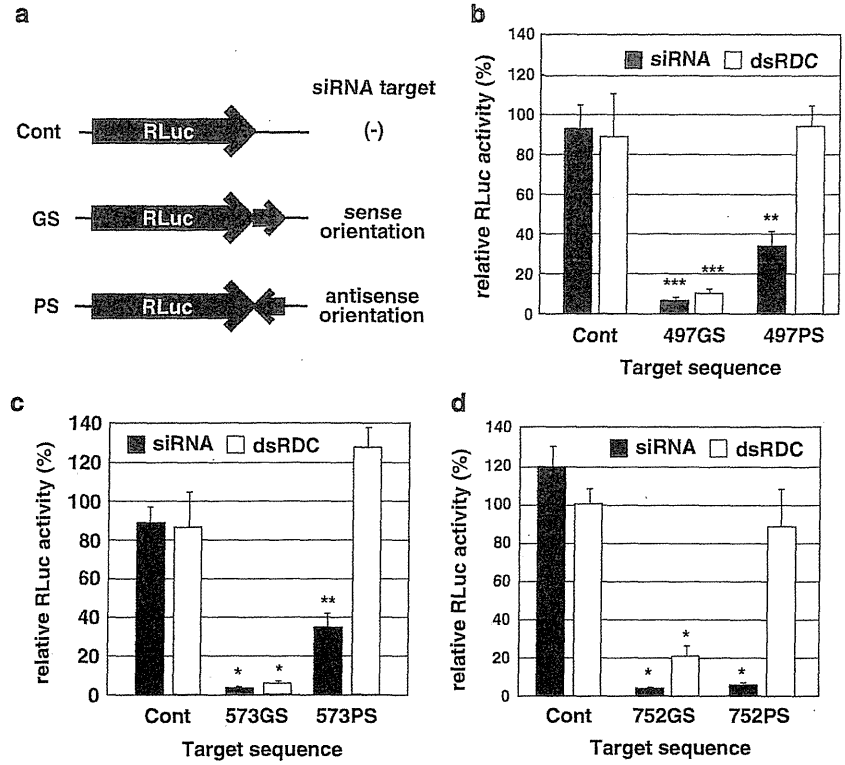

Figure 3 Lack of passenger-strand mediated RNA interference (RNAi) in E6E7 double-strand RNA–DNA chimera (dsRDC). Plasmids ligated with a small interfering RNA (siRNA) target sequence in a sense orientation (497GS, 573GS and 752GS) expressed targets of the guide strand (GS)-loaded RNA-induced silencing complex (RISC), whereas those in an antisense orientation (497PS, 573PS and 752PS) expressed targets of the passenger strand (PS)-loaded RISC (**a**). HeLa cells were co-transfected with *Renilla* luciferase (RLuc)-GS (497GS, 573GS and 752GS) or RLuc-PS expression plasmids (497PS, 573PS and 752PS), along with respective siRNA and dsRDC (497 (**b**), 573 (**c**) and 752 (**d**)). Data points marked with asterisks are statistically significant as compared with control transfection (*$P<0.001$; **$P<0.01$; ***$P<0.05$). All siRNAs examined here exhibited PS- and GS-mediated RNAi, whereas all examined dsRDCs showed only GS-mediated RNAi.

Lack of PS-mediated RNAi in E6E7 dsRDCs

To examine the differences between E6E7 siRNAs and their dsRDC forms with regard to PS-mediated silencing activity, we used an expression plasmid comprised of RLuc fused with 23-bp siRNA target sequences in sense and antisense directions as GS and PS targets, respectively (Figure 3a). As shown in Figure 3b–d, all siRNAs tested (497, 573 and 752) suppressed their respective RLuc-GS as well as RLuc-PS expression, whereas their dsRDC counterparts suppressed only RLuc-GS.

Effects of HPV16 E6E7 siRNAs and dsRDCs on off-target candidate genes

We also examined whether 6-nucleotide DNA substitution in the seed region (nucleotides 1–6 from the 5′ end of GS) could alter the off-target property of siRNA towards human gene sequences with 3-nucleotide mismatches to each E6E7 siRNA GS (Table 1), using plasmids of RLuc fused with 19-bp off-target candidate gene sequences (OT). HeLa cells were transfected with siRNA or dsRCD (2 nM) along with a corresponding RLuc-OT plasmid, and then analyzed using a dual luciferase assay. E6E7 siRNAs and dsRDCS showed no or very mild inhibitory effects on 7 of 10 sequences with less than 35% suppression (data not shown). Furthermore, 497OT-2 was inhibited by siRNA-497 to 23.6%, whereas its suppression by dsRDC-497 was significantly less (65.6%, $P<0.001$; Figure 4a), indicating that dsRDC modification of 497 reduced off-target activity. In addition, 573OT-2 and 573OT-3 expressions were suppressed by siRNA-573 to 20.3 and 49.5%, respectively. Surprisingly, dsRDC modification of siRNA-573 did not reduce the inhibitory effect on 573OT-2 or OT-3 (Figure 4b and c).

Next, we examined whether E6E7 siRNA (497 and 573) could suppress mRNA expression of the off-target candidate genes (497OT-2, *POU4F1*; 573OT-2, AL832149; 573OT-3, *GTF2H4*) using quantitative reverse transcription-PCR. As neither SiHa nor HeLa cells expressed *POU4F1*, we used SNU-1 cells, which expressed all three OT genes. SNU-1 cells were transfected with siRNA-497 or dsRDC-497 for 2 days, and then analyzed for mRNA expression of *POU4F1* (Figure 4d). siRNA-497 suppressed the *POU4F1* mRNA level to 57.7%, whereas dsRDC-497 had no effect. The mRNA levels were parallel to RLuc activities of 497OT-2 (Figure 4a). Similarly, the effects of siRNA-573 and its dsRDC form on AL8321449 mRNA level were examined using SNU-1 cells (Figure 4e). siRNA-573 decreased its level to 65.4% and

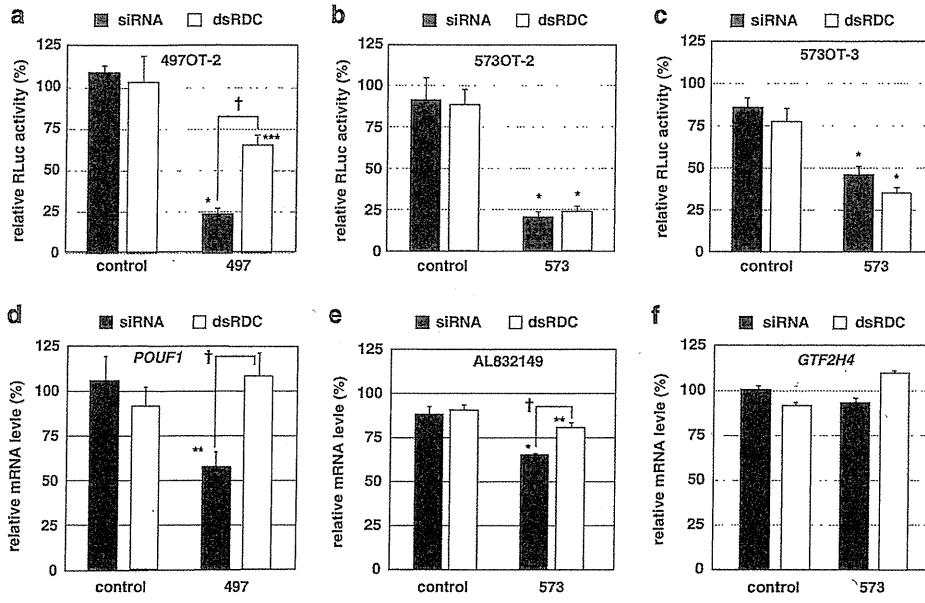

Figure 4 Effects of human papillomavirus 16 (HPV16) E6E7 small interfering RNA (siRNA) and double-strand RNA–DNA chimera (dsRDC) on off-target candidate sequences. All human gene sequences carrying 3-nucleotide mismatches to the guide strand (nucleotides 1–19 from the 5′ end) of E6E7 siRNAs are listed in Table 1. The 23-nucleotides oligoDNAs encompassing these 19-nucleotide sequences were synthesized and ligated downstream to the stop codon of *Renilla* luciferase (RLuc) in a psiCheck2 plasmid. HeLa cells were co-transfected with RLuc-497OT-2 (**a**) or RLuc-573OT-2 (**b**), or an RLuc-573OT-3 expression plasmid (**c**), along with respective siRNAs and their dsRDC counterparts (2 nM). After 48 h of incubation, cells were analyzed using a dual luciferase assay. RLuc activities were normalized to those of firefly luciferase (FLuc). RLuc activities relative to mock-transfected cells are shown. SNU-1 cells transfected with siRNAs (473 and 573) and their dsRDC counterparts at 100 nM were incubated for 48 h, and then analyzed for 497OT-2 (*POU4F1*, **d**), 573OT-2 (AL832149, **e**) and 573OT-3 (*GTF2H4*, **f**) expressions using quantitative reverse transcription-PCR (qRT-PCR). mRNA levels were normalized to that of 18S rRNA and those relative to mock-transfected cells are shown. All experiments were performed in triplicate and error bars represent the standard deviation from the mean. Data points marked with asterisks are statistically significant as compared with control transfection ($^{*}P<0.001$; $^{**}P<0.01$; $^{***}P<0.05$). Data points marked with crosses are statistically significant ($^{\dagger}P<0.01$).

dsRDC modification partially relieved the suppression (80.8%). *GTF2H4* mRNA expression was unaffected by siRNA-573 and its dsRDC form (91.9 and 93.4%, respectively; Figure 4f), whereas expression of 573OT-3 carrying the same target sequence was inhibited by more than twofold (Figure 4c), suggesting that *GTF2H4* mRNA might have lower accessibility to RNA-induced silencing complex than artificial 573OT-3 mRNA. These results showed that E6E7 siRNA exerts off-target effects toward some human genes carrying 3-nucleotide mismatches to siRNA and that dsRDC modification can reduce the off-target effects of some, if not all, mRNAs.

Effects of HPV16 E6E7 siRNAs and dsRDC on growth of E6E7-positive and -negative keratinocytes

Finally, we examined whether E6E7 dsRDC (497) suppressed the growth of E6E7-immortalized keratinocytes (HDK1-E6E7) with features of early cervical cancer cells.[31] *TERT*-immortalized keratinocytes (HDK1-T) were used as an E6E7-negative control. The vulnerability of these cells to FLuc siRNA transfection was tested using HDK1-E6E7-luc and HDK1-T-luc. The dose effect of FLuc siRNA on FLuc activity was similar between the cells at concentrations of 0.004–1.0 nM (data not shown), indicating that these cells could be transfected with siRNA to induce target gene silencing with comparable efficacy.

HDK1-E6E7-luc and HDK1-T-luc cells were transfected with control and E6E7 siRNAs, as well as their dsRDC-modified forms (497 and 752) at 0.5 nM for 6 days. A WST8 assay did not reflect a viable cell number of E6E7 siRNA-treated HDK1-E6E7 cells (data not shown), thus we took advantage of the constitutive FLuc expression of these cells and relative cell viability was determined based on FLuc activity, which paralleled cell viability. As shown in Figure 5a and b, siRNA-497 suppressed the growth of *TERT*-immortalized keratinocytes as well as E6E7-immoratalized keratinocytes, indicating that siRNA-497 had nonspecific growth suppression, as also seen in FL-HeLa-1 cells (Figure 2b). When siRNA-497 was modified to a dsRDC form, nonspecific growth inhibition of HDK1-T-luc was reduced and cell viability recovered to 62.5%, with a marginal loss of growth suppression of E6E7-immortalized cells (19.1%). siRNA-752 also showed specific growth suppression as compared with siRNA control and siRNA-497. However, dsRDC modification compromised the E6E7-specific growth suppression of siRNA-752. Taken together,

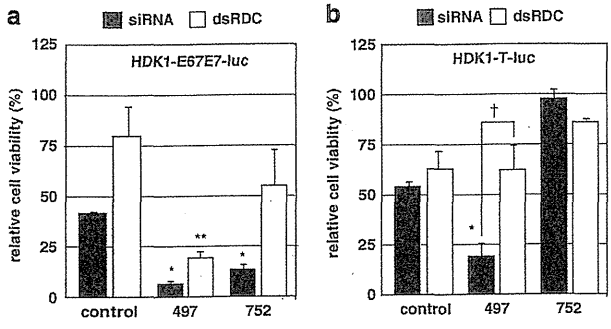

Figure 5 Specific growth suppression of E6E7-immortalized human keratinocytes by E6E7 double-strand RNA–DNA chimeras (dsRDCs). Human papillomavirus 16 (HPV16) E6E7-immortalized keratinocytes (HDK1-E6E7) and *TERT*-immortalized (HDK1-T) stably expressing luciferase were obtained, and designated as HDK1-E6E7-luc and HDK1-T-luc, respectively. HDK1-E6E7-luc (**a**) and HDK1-T-luc (**b**) cells were transfected with mock, small interfering RNA (siRNA) (control, 497 and 752) or their dsRDC counterparts at 0.5 nM. At 5 days after transfection, relative cell viability was determined using a luciferase assay. Data points marked with asterisks are statistically significant as compared with control transfection ($^{*}P<0.001$; $^{**}P<0.01$). Data points marked with crosses are statistically significant ($^{\dagger}P<0.01$).

these results showed that dsRDC-497 and siRNA-752 are able to induce specific growth suppression of E6E7-expressing keratinocytes.

Discussion

In this study, we assessed the off-target activities of E6E7 siRNAs (497, 573 and 752) and their dsRDC modified forms using 10 potential human off-target sequences carrying 3-nucleotide mismatches to the GS of E6E7 siRNA (nucleotides 1–19 from the 5′ end). In most cases, 3-nucleotide mismatches were adequate to avoid suppression of artificial mRNA of RLuc fused with a single copy of the off-target candidate sequence. However, the silencing effect was significant when targeted mRNA contained a single copy of the 19-nucleotide sequence with a completely matched seed region as well as one of three mismatches located at either nucleotide 1 or 19 from the 5′ end of the GS. These sequences (497OT-2, 573OT-2 and 573OT-3) were found to have mismatches to their respective siRNAs at position 10, or at positions 10 and 11 from the 5′ end of the GS. Pairing of these GS nucleotides to target mRNA is essential for mRNA cleavage and mismatch of these positions is a hallmark of miRNA-mediated translational inhibition.[32–34] Thus, the off-target effects observed in our study might have been mediated through miRNA-like activity without mRNA cleavage.

Perfect RNA–RNA duplex formation between the siRNA seed region (GS positions 2–8 from the 5′ end) and unintended target mRNA is essential for off-target silencing.[3,5,6] Using unmodified authentic siRNA, we previously found that the melting temperatures of seed–mRNA duplexes (T_m 2–8) are divergent and positively correlated to the extent of off-target suppression.[35] We also reported that this rule is applicable to the off-target effects mediated by dsRDCs.[36] Substitution of seed RNA by DNA lowers T_m 2–8, which explains why most dsRDCs, if not all, might have reduced off-target effects as compared with siRNA.[8] In this study, dsRDC modification reduced the inhibitory effects of siRNA-497 on RLuc-497OT-2 and *POU4F1* mRNA expressions, which was consistent with our previous observation.[8,36] In contrast, similar DNA substitution of siRNA-573 did not compromise the suppression of RLuc-573OT-2. According to results of our calculation formula,[35] the T_m 2–8 change induced by dsDNA modification was highest in siRNA-497 (11.5 °C), followed by siRNA-752 (7.7 °C) and lowest in siRNA-573 (6.9 °C), which was well correlated with their reduction of off-target effects.

All HPV16 E6E7 siRNAs (497, 573 and 752) showed potent nonspecific cytotoxicity in HeLa-derived cells cultured at a low density. As HeLa cells express HPV18 E6E7 mRNAs with a relatively low homology to HPV16 E6E7 mRNAs, we analyzed the HPV18 E6E7 region and found no sequences perfectly matching the seed regions of these siRNAs, which is the minimal requirement for knockdown of HPV18 E6E7 (data not shown).[3,5,6] Control siRNA also exhibited cytotoxicity to FL-HeLa-1 cells under the same conditions. Furthermore, siRNA (497) was highly toxic to *TERT*-immortalized keratinocytes lacking E6E7 expression. Thus, these results suggested that the nonspecific cytotoxicity of these siRNAs was not mediated through suppression of E6E7 in FL-HeLa-1 cells. Reduction of off-target effects by dsDNA modification was correlated with their reduction of cytotoxicity. These results favor the hypothesis that nonspecific cytotoxicity is induced by off-target suppression of genes that regulate cell growth and viability.[7] Alternatively, such cytotoxicity might be mediated by disturbing the endogenous miRNA pathways through competition of molecules involved in RNAi by exogenous siRNA.[10–12] It remains to be determined how siRNA exerts toxic effects in transduced cells.

We previously reported that most E6E7 siRNAs, with a few exceptions including 573,[8] exerted PS-mediated silencing toward mRNA containing inverted E6E7 (628 bp fragment). However, we detected PS-mediated silencing in all siRNAs (497, 753 and 573) tested in this study when mRNAs containing inverted short target sequences were used as targets. Detection of PS RNAi might be influenced by the secondary structure of the target mRNA. Our results suggest that PS RNAi is unavoidable in conventional siRNAs. Thus, modifications such as dsRDC would be applicable for avoiding unwanted PS-induced silencing.

Deregulation of E6 and E7 expression is an initial event during multistep carcinogenesis in cervical cancer. In addition to expressions of these oncogenes, progression into overt cancer requires additional genetic changes. Human keratinocytes immortalized with HPV16 E6E7 were shown to be less invasive and have a less tumorigenic phenotype.[31] Using E6E7-immortalized keratinocytes as

an early disease model and *TERT*-immortalized keratinocyte s as normal keratinocytes, we examined the effects of E6E7 siRNA and dsRDC on their growth and specificity, and found that dsRDC-497 and siRNA-752 suppressed the growth of E6E7-positive keratinocytes, but not that of E6E7-negative keratinocytes. Thus, those might be useful for the treatment of pre-cancer and early cancer lesions.

In summary, we found that dsRDC modification enhanced the specificity of HPV16 E6E7 siRNA by reducing its nonspecific cytotoxicity and off-target property. E6E7 dsRDC inhibited the growth of E6E7-expressing human keratinocytes as well as HPV16-positive cervical cancer cells; however, not that of non-expressing keratinocytes. Taken together, our results indicate a large potential for HPV16 E6E7 dsRDC in treatments for HPV16-related cancer and early disease stages.

Conflicts of interest

The authors declare no conflicts of interest.

Acknowledgements

We thank Yukikazu Natori (Tokyo Institute of Technology) for the helpful discussion and suggestions. This work was supported in part by Grant-in-Aid for Scientific Research from the Japan Society for the Promotion of Science (KY) and a Grant-in-Aid for Cancer Research from the Ministry of Health Labor and Welfare of Japan (KY).

References

1 Elbashir SM, Harborth J, Lendeckel W, Yalcin A, Weber K, Tuschl T. Duplexes of 21-nucleotide RNAs mediate RNA interference in cultured mammalian cells. *Nature* 2001; **411**: 494–498.
2 Caplen NJ, Parrish S, Imani F, Fire A, Morgan RA. Specific inhibition of gene expression by small double-stranded RNAs in invertebrate and vertebrate systems. *Proc Natl Acad Sci USA* 2001; **98**: 9742–9747.
3 Jackson AL, Bartz SR, Schelter J, Kobayashi SV, Burchard J, Mao M *et al.* Expression profiling reveals off-target gene regulation by RNAi. *Nat Biotechnol* 2003; **21**: 635–637.
4 Saxena S, Jonsson ZO, Dutta A. Small RNAs with imperfect match to endogenous mRNA repress translation. Implications for off-target activity of small inhibitory RNA in mammalian cells. *J Biol Chem* 2003; **278**: 44312–44319.
5 Lin X, Ruan X, Anderson MG, McDowell JA, Kroeger PE, Fesik SW *et al.* siRNA-mediated off-target gene silencing triggered by a 7 nt complementation. *Nucleic Acids Res* 2005; **33**: 4527–4535.
6 Birmingham A, Anderson EM, Reynolds A, Ilsley-Tyree D, Leake D, Fedorov Y *et al.* 3′ UTR seed matches, but not overall identity, are associated with RNAi off-targets. *Nat Methods* 2006; **3**: 199–204.
7 Jackson AL, Burchard J, Leake D, Reynolds A, Schelter J, Guo J *et al.* Position-specific chemical modification of siRNAs reduces 'off-target' transcript silencing. *RNA* 2006; **12**: 1197–1205.
8 Ui-Tei K, Naito Y, Zenno S, Nishi K, Yamato K, Takahashi F *et al.* Functional dissection of siRNA sequence by systematic DNA substitution: modified siRNA with a DNA seed arm is a powerful tool for mammalian gene silencing with significantly reduced off-target effect. *Nucleic Acids Res* 2008; **36**: 2136–2151.
9 Bramsen JB, Laursen MB, Nielsen AF, Hansen TB, Bus C, Langkjaer N *et al.* A large-scale chemical modification screen identifies design rules to generate siRNAs with high activity, high stability and low toxicity. *Nucleic Acids Res* 2009; **37**: 2867–2881.
10 Castanotto D, Sakurai K, Lingeman R, Li H, Shively L, Aagaard L *et al.* Combinatorial delivery of small interfering RNAs reduces RNAi efficacy by selective incorporation into RISC. *Nucleic Acids Res* 2007; **35**: 5154–5164.
11 Grimm D, Streetz KL, Jopling CL, Storm TA, Pandey K, Davis CR *et al.* Fatality in mice due to oversaturation of cellular microRNA/short hairpin RNA pathways. *Nature* 2006; **441**: 537–541.
12 Khan AA, Betel D, Miller ML, Sander C, Leslie CS, Marks DS. Transfection of small RNAs globally perturbs gene regulation by endogenous microRNAs. *Nat Biotechnol* 2009; **27**: 549–555.
13 Bosch FX, de Sanjose S. Chapter 1: Human papillomavirus and cervical cancer—burden and assessment of causality. *J Natl Cancer Inst Monogr* 2003; **31**: 3–13.
14 zur Hausen H. Papillomaviruses causing cancer: evasion from host-cell control in early events in carcinogenesis. *J Natl Cancer Inst* 2000; **92**: 690–698.
15 Longworth MS, Laimins LA. Pathogenesis of human papillomaviruses in differentiating epithelia. *Microbiol Mol Biol Rev* 2004; **68**: 362–372.
16 Munger K, Baldwin A, Edwards KM, Hayakawa H, Nguyen CL, Owens M *et al.* Mechanisms of human papillomavirus-induced oncogenesis. *J Virol* 2004; **78**: 11451–11460.
17 Yugawa T, Kiyono T. Molecular mechanisms of cervical carcinogenesis by high-risk human papillomaviruses: novel functions of E6 and E7 oncoproteins. *Rev Med Virol* 2009; **19**: 97–113.
18 Chen Z, Kamath P, Zhang S, St John L, Adler-Storthz K, Shillitoe EJ. Effects on tumor cells of ribozymes that cleave the RNA transcripts of human papillomavirus type 18. *Cancer Gene Ther* 1996; **3**: 18–23.
19 Venturini F, Braspenning J, Homann M, Gissmann L, Sczakiel G. Kinetic selection of HPV 16 E6/E7-directed antisense nucleic acids: anti-proliferative effects on HPV 16-transformed cells. *Nucleic Acids Res* 1999; **27**: 1585–1592.
20 DeFilippis RA, Goodwin EC, Wu L, DiMaio D. Endogenous human papillomavirus E6 and E7 proteins differentially regulate proliferation, senescence, and apoptosis in HeLa cervical carcinoma cells. *J Virol* 2003; **77**: 1551–1563.
21 Jiang M, Milner J. Selective silencing of viral gene expression in HPV-positive human cervical carcinoma cells treated with siRNA, a primer of RNA interference. *Oncogene* 2002; **21**: 6041–6048.
22 Yoshinouchi M, Yamada T, Kizaki M, Fen J, Koseki T, Ikeda Y *et al. In vitro* and *in vivo* growth suppression of human papillomavirus 16-positive cervical cancer cells by E6 siRNA. *Mol Ther* 2003; **8**: 762–768.
23 Butz K, Ristriani T, Hengstermann A, Denk C, Scheffner M, Hoppe-Seyler F. siRNA targeting of the viral E6 oncogene efficiently kills human papillomavirus-positive cancer cells. *Oncogene* 2003; **22**: 5938–5945.

24 Hall AH, Alexander KA. RNA interference of human papillomavirus type 18 E6 and E7 induces senescence in HeLa cells. *J Virol* 2003; **77**: 6066–6069.
25 Bosch FX, Castellsague X, de Sanjose S. HPV and cervical cancer: screening or vaccination? *Br J Cancer* 2008; **98**: 15–21.
26 Putral LN, Bywater MJ, Gu W, Saunders NA, Gabrielli BG, Leggatt GR *et al.* RNA interference against human papillomavirus oncogenes in cervical cancer cells results in increased sensitivity to cisplatin. *Mol Pharmacol* 2005; **68**: 1311–1319.
27 Yamato K, Yamada T, Kizaki M, Ui-Tei K, Natori Y, Fujino M *et al.* New highly potent and specific E6 and E7 siRNAs for treatment of HPV16 positive cervical cancer. *Cancer Gene Ther* 2008; **15**: 140–153.
28 Haga K, Ohno S, Yugawa T, Narisawa-Saito M, Fujita M, Sakamoto M *et al.* Efficient immortalization of primary human cells by p16INK4a-specific short hairpin RNA or Bmi-1, combined with introduction of hTERT. *Cancer Sci* 2007; **98**: 147–154.
29 Naito Y, Yamada T, Ui-Tei K, Morishita S, Saigo K. siDirect: highly effective, target-specific siRNA design software for mammalian RNA interference. *Nucleic Acids Res* 2004; **32**: W124–W129.
30 Lanham S, Herbert A, Watt P. HPV detection and measurement of HPV-16, telomerase, and survivin transcripts in colposcopy clinic patients. *J Clin Pathol* 2001; **54**: 304–308.
31 Narisawa-Saito M, Yoshimatsu Y, Ohno S, Yugawa T, Egawa N, Fujita M *et al.* An *in vitro* multistep carcinogenesis model for human cervical cancer. *Cancer Res* 2008; **68**: 5699–5705.
32 Hutvagner G, Zamore PD. A microRNA in a multiple-turnover RNAi enzyme complex. *Science* 2002; **297**: 2056–2060.
33 Doench JG, Petersen CP, Sharp PA. siRNAs can function as miRNAs. *Genes Dev* 2003; **17**: 438–442.
34 Chiu YL, Rana TM. RNAi in human cells: basic structural and functional features of small interfering RNA. *Mol Cell* 2002; **10**: 549–561.
35 Ui-Tei K, Naito Y, Nishi K, Juni A, Saigo K. Thermodynamic stability and Watson–Crick base pairing in the seed duplex are major determinants of the efficiency of the siRNA-based off-target effect. *Nucleic Acids Res* 2008; **36**: 7100–7109.
36 Ui-Tei K, Nishi K, Naito Y, Zenno S, Juni A, Saigo K. Reduced base–base interactions between the DNA seed and RNA target are the major determinants of a significant reduction in the off-target effect due to DNA-seed-containing siRNA. *Proceedings of the 2009 Micro-Nano Mechatronics and Human Science*; 2009, pp 298–304.

Supplementary Information accompanies the paper on Cancer Gene Therapy website (http://www.nature.com/cgt)